



## Research paper



## Molecular design, synthesis and anticancer activity of new thiopyrano [2,3-*d*]thiazoles based on 5-hydroxy-1,4-naphthoquinone (juglone)

Iryna Ivasechko<sup>a,1</sup>, Andrii Lozynskiy<sup>b,1</sup>, Julia Senkiv<sup>a,1</sup>, Piotr Roszczenko<sup>c</sup>, Yuliia Kozak<sup>a</sup>, Nataliya Finiuk<sup>a</sup>, Olga Klyuchivska<sup>a</sup>, Nataliya Kashchak<sup>a</sup>, Nazar Manko<sup>a</sup>, Zvenyslava Maslyak<sup>k</sup>, Danylo Lesyk<sup>b</sup>, Andriy Karkhut<sup>d</sup>, Svyatoslav Polovkovych<sup>d</sup>, Robert Czarnomysy<sup>e</sup>, Olga Szewczyk<sup>e</sup>, Andriy Kozytskiy<sup>f,8</sup>, Olexandr Karpenko<sup>f</sup>, Dmytro Khylyuk<sup>h</sup>, Andrzej Gzella<sup>i</sup>, Krzysztof Bielawski<sup>e</sup>, Anna Bielawska<sup>c</sup>, Petr Dzubak<sup>l</sup>, Sona Gurska<sup>l</sup>, Marian Hajduch<sup>l</sup>, Rostyslav Stoika<sup>a,\*\*</sup>, Roman Lesyk<sup>b,j,\*</sup>

<sup>a</sup> Institute of Cell Biology of National Academy of Sciences of Ukraine, Drahomanov14/16, Lviv, 79005, Ukraine

<sup>b</sup> Department of Pharmaceutical, Organic and Bioorganic Chemistry, Danylo Halytsky Lviv National Medical University, Pekarska 69, Lviv, 79010, Ukraine

<sup>c</sup> Department of Biotechnology, Faculty of Pharmacy, Medical University of Białystok, Jana Kilińskiego 1, 15-089, Białystok, Poland

<sup>d</sup> Department of Technology of Biologically Active Substances, Pharmacy and Biotechnology, Lviv Polytechnic National University, Bandera 12, Lviv, 79013, Ukraine

<sup>e</sup> Department of Synthesis and Technology of Drugs, Faculty of Pharmacy, Medical University of Białystok, Jana Kilińskiego 1, 15-089, Białystok, Poland

<sup>f</sup> Enamine Ltd, Chervonotkatska Street 78, Kyiv, 02094, Ukraine

<sup>8</sup> L. V. Pysarzhevsky Institute of Physical Chemistry, National Academy of Sciences of Ukraine, Nauky Avenue 31, Kyiv, 03028, Ukraine

<sup>h</sup> Department of Organic Chemistry, Faculty of Pharmacy with Medical Analytics Division, Medical University of Lublin, 4A Chodzki, Lublin, 20-093, Poland

<sup>i</sup> Department of Organic Chemistry, Poznan University of Medical Sciences, Grunwaldzka 6, 60-780, Poznan, Poland

<sup>j</sup> Department of Biotechnology and Cell Biology, Medical College, University of Information Technology and Management in Rzeszow, Sucharskiego 2, 35-225, Rzeszow, Poland

<sup>k</sup> Institute of Blood Pathology and Transfusion Medicine of National Academy of Medical Sciences of Ukraine, General Chupryny 45, Lviv, 79044, Ukraine

<sup>l</sup> Institute of Molecular and Translational Medicine, Faculty of Medicine and Dentistry, Palacky University and University Hospital in Olomouc, Hnevotinska 5, 77900, Olomouc, Czech Republic

## ARTICLE INFO

Handling Editor: Dr. Z Liu

## Keywords:

Drug design

Juglone

Thiopyranothiazoles

Anticancer activity

DNA interaction

Apoptosis

Molecular docking

## ABSTRACT

A series of 11-substituted 9-hydroxy-3,5,10,11-tetrahydro-2*H*-benzo[6,7]thiochromeno[2,3-*d*][1,3]thiazole-2,5,10-triones **3.1**–**3.13** were synthesized via *hetero*-Diels-Alder reaction of 5-ene-4-thioxo-2-thiazolidinones and 5-hydroxy-1,4-naphthoquinone (juglone). The structure of newly synthesized compounds was established by means of spectral data and a single-crystal X-ray diffraction analysis. The synthesized compounds were tested on a panel of cell lines representing different types of cancer as well as normal and pseudonormal cells and peripheral human blood lymphocytes. Compound **3.10** was found to be the most active derivative, exhibiting a cytotoxic effect similar to doxorubicin's one (IC<sub>50</sub> ranged from 0.6 to 5.98 μM), but less toxic to normal and pseudonormal cells. All synthesized compounds were able to interact with DNA, although their anticancer activity did not correlate with the potency of interaction with DNA. The status of p53 in colorectal cancer cells correlated with the activity of the synthesized derivatives **3.1**, **3.7**, and **3.10**. Compound **3.10** did not have an acute toxic effect on the body of C57BL/6 mice, unlike the well-known anticancer drug doxorubicin, which was used as a positive control. The injection of **3.10** (20 mg/kg) to mice had no effect on the counts of leukocytes, erythrocytes, platelets and hemoglobin level in their blood, in contrast to doxorubicin, which caused anemia and leukopenia, indicating bio-tolerance of **3.10** *in vivo*.

\* Corresponding author. Department of Pharmaceutical, Organic and Bioorganic Chemistry, Danylo Halytsky Lviv National Medical University, Pekarska 69, Lviv, 79010, Ukraine.

\*\* Corresponding author.

E-mail addresses: [stoika.rostyslav@gmail.com](mailto:stoika.rostyslav@gmail.com) (R. Stoika), [dr\\_r\\_lesyk@org.lviv.net](mailto:dr_r_lesyk@org.lviv.net) (R. Lesyk).

<sup>1</sup> equal contribution.

<https://doi.org/10.1016/j.ejmech.2023.115304>

Received 21 February 2023; Received in revised form 20 March 2023; Accepted 22 March 2023

Available online 24 March 2023

0223-5234/© 2023 The Authors. Published by Elsevier Masson SAS. This is an open access article under the CC BY-NC-ND license (<http://creativecommons.org/licenses/by-nc-nd/4.0/>).

## 1. Introduction

A design of new drugs is time-consuming and multi-stage process that continues for years and requires big financial costs. A key stage in this process is connected with medicinal chemistry, namely a search and optimization of the lead compounds. The identification of these compounds is the starting point for obtaining molecules with required activity, selectivity of action and acceptable parameters of ADMET (adsorption, distribution, metabolism, elimination, and toxicity). As a source of lead compounds, one can use endogenous ligands, particularly substrates of enzymes, transport proteins, or receptor agonists, as well as other ligands, including existing drugs, compounds isolated from drug metabolic pathways, or compounds undergoing clinical trials. Besides, these may be compounds identified through screening studies, including the compounds of natural origin [1].

It is worth noting that thiazole and its structure-related analogs thiazolidinone derivatives constitute a known class of compounds that can become the basis for the creation of novel lead compounds, since they have a broad spectrum of the biological activities and great potential for further chemical modification. The thiazole/thiazolidinone core underlies numerous compounds of natural origin that exhibit pharmacological activity, namely, the glycoside antitumor antibiotics, macrolides, cyclic and linear peptides, depsipeptide and diterpenes have been already registered as drugs or derivatives that are on the stages of pre-clinical trials. In addition, thiazole/thiazolidinone derivatives are the basement of numerous synthetic drugs with different biological activities (Fig. 1) [2–4].

Among thiazole/thiazolidinone-based derivatives, their fused analogs, for example thiopyrano[2,3-*d*]thiazoles, also deserve a particular pharmacological interest [5]. Thus, thiopyrano[2,3-*d*]thiazoles with anticancer [6], antimycobacterial [7], anti-inflammatory [8], antiviral [9] and antitrypanosomal [10] properties have been identified. Several approaches for obtaining thiopyrano[2,3-*d*]thiazole derivatives have been described, for instance, the *hetero*-Diels-Alder reaction of 5-ene-4-thio-2-thiazolidinones (5-ene-isorhodanines) with different dienophiles, Michael reaction with activated nitriles, as well as the reaction of 4-thio-2-thiazolidinone and *ortho*-substituted aldehydes in the Knoevenagel condensation [11–14].

1,4-Naphthoquinone-based derivatives is another group of considerable attention in modern medicinal chemistry that also occur in nature. The naphthoquinones have demonstrated a broad range of

biological activities, such as antioxidant [15,16], anti-inflammatory [17], anticancer [18–20], antifungal [21], and antitrypanosomal [22]. Among them, the juglone (5-hydroxy-1,4-naphthoquinone) deserves a particular interest [23]. It is a natural compound that is widely spread in several *Juglandaceae* members, less often in *Proteaceae*, *Caesalpiniaceae*, and *Fabaceae*. Juglone was reported to possess anticancer, antioxidant, repellent, antiparasitic, antifungal, and allelopathic properties, as well as sedative effects in vertebrates [24–27]. In addition, the juglone's cytotoxic effects on human cell lines were characterized by a reduction of level of p53 protein [28], DNA damage, inhibition of transcription [29], and induction of cell death [30]. Furthermore, this nature compound utilizes different mechanisms of anticancer activity via Pin1 inhibition [31], blocking the S-phase of cell cycle [32], increasing intracellular Ca<sup>2+</sup> concentration, inducing mitochondria-dependent apoptosis pathways, rupture of outer mitochondrial-membrane, reducing expression of the anti-apoptotic Bcl-2 [24] and activating pro-apoptotic caspase-9 and caspase-3 [33].

The goal of our study was the synthesis of condensed hybrid 4-thiazolidinone derivatives, namely thiopyrano[2,3-*d*]thiazole with the juglone fragment in structure via the *hetero*-Diels-Alder reaction (Fig. 2). The synthesized compounds were evaluated for their anticancer activity *in vitro*, DNA interaction, as well as general toxicity *in vivo*.

## 2. Results and discussion

Based on our previous studies of thiopyranothiazoles with a naphthoquinone moiety [34], we synthesized new derivatives via a *hetero*-Diels-Alder reaction of the juglone (5-hydroxy-1,4-naphthoquinone) **1** as dienophile and 5-ene-4-thio-2-thiazolidinones **2**, as heterodienes (see Scheme 1). Starting compounds (5-ene-isorhodanines) **2.1–2.11** were obtained in high yield through Knoevenagel condensation of isorhodanine with aldehydes or ketones [35]. In addition, the synthesis of 11-(furan-2-yl)-3,11-dihydro-2*H*-benzo[6,7]thiochromeno[2,3-*d*]thiazole-2,5,10-trione **3.11** as structurally related analog to compound **3.10** was carried out via *hetero*-Diels-Alder reaction of 5-(furan-2-ylmethylene)-4-thio-2-thiazolidinone as heterodiene and 1,4-naphthoquinone as a dienophile. The synthesis of compound **3.13** was accomplished via reaction of isorhodanine, 3-phenylpropionaldehyde and 5-hydroxy-1,4-naphthoquinone in acetonitrile in the presence of EDDA as a catalyst.

There are many reports that the Diels-Alder reaction of asymmetric

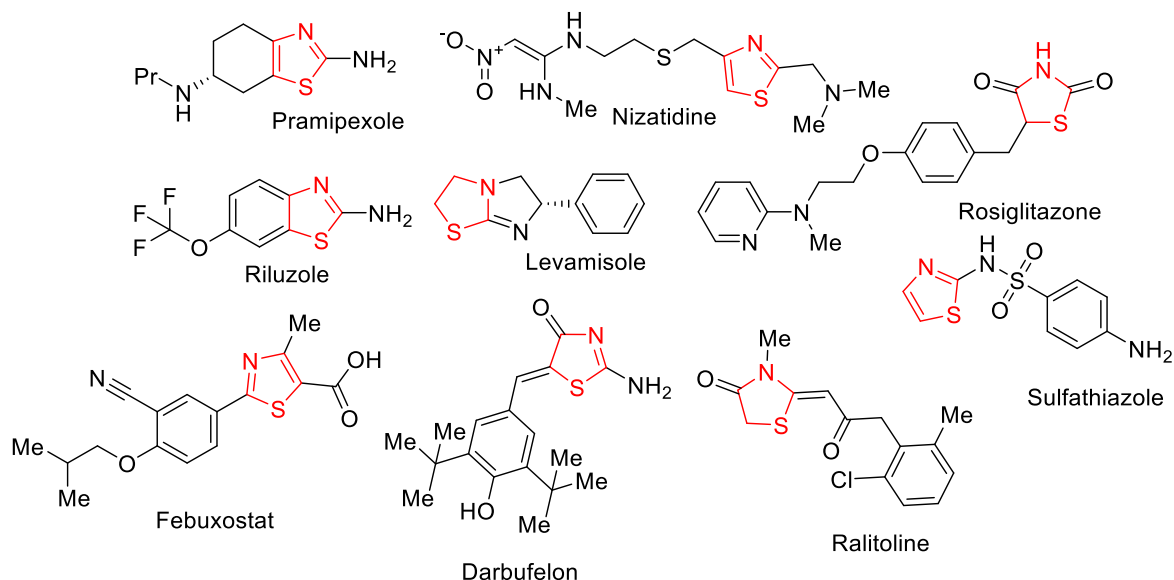


Fig. 1. Structures of thiazole/thiazolidinone-bearing drugs.

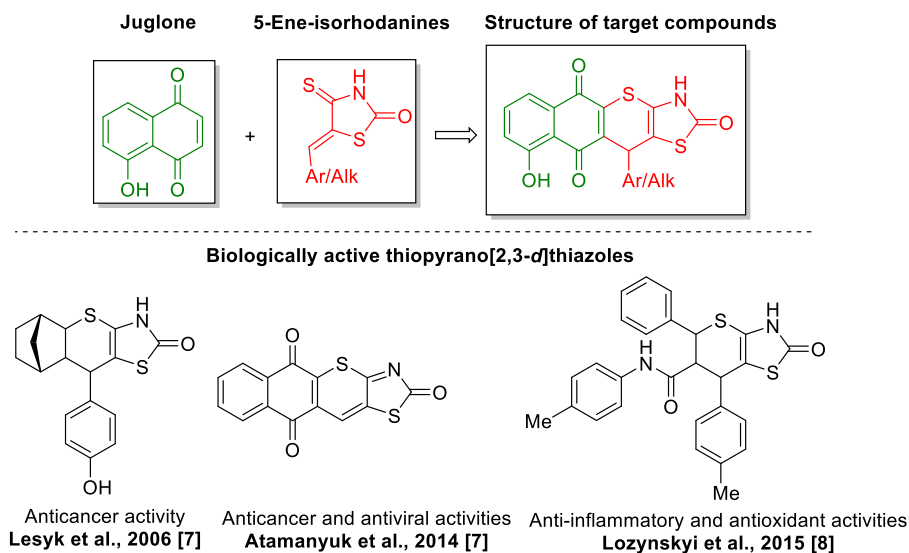
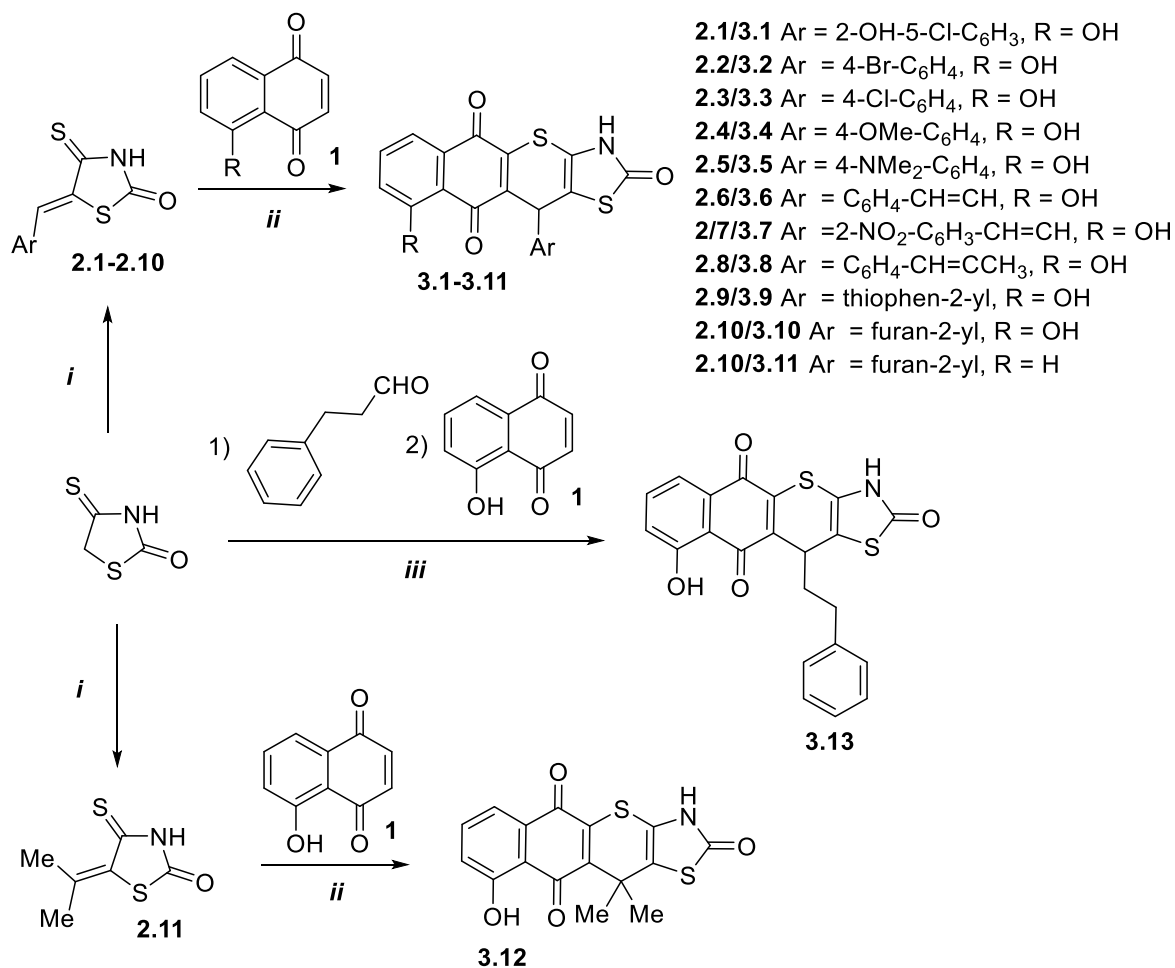


Fig. 2. Design of the target compounds.



**Scheme 1.** Synthesis of target thiopyranthiazoles with a naphthoquinone moiety. *Reagents and conditions:* i) 4-thio-2-thiazolidinone (isorhodanine) (10 mmol), aldehyde or ketone (11 mmol), EDDA (5 μmol), EtOH (10 ml), reflux, 10 min, 70–90%; ii) 5-ene-4-thio-2-thiazolidinone (10 mmol), 1,4-naphthoquinone or 5-hydroxy-1,4-naphthoquinone (20 mmol), hydroquinone (5 μmol), AcOH (10 ml), reflux, 1 h, 62–79%; iii) isorhodanine (5.0 mmol), phenylpropionaldehyde (5.5 mmol), 5-hydroxy-1,4-naphthoquinone (10 mmol), EDDA (5.0 μmol), MeCN (10 ml), reflux, 2 h, 65%.

naphthoquinone derivatives as dienophiles undergoes via an absence of a regioselective process [36–38]. However, trapping 5-ene-4-thioxo-2-thiazolidinones **2** with 5-hydroxy-1,4-naphthoquinone led to only a single tetracyclic quinone regio-isomer (9-hydroxy isomer), where 6-hydroxy isomer was not isolated.

The structure of the synthesized compounds was elucidated through analysis of spectral data. In the  $^1\text{H}$  NMR spectra of the synthesized thiopyranthiazoles, a characteristic sub-spectrum of protons of the naphthoquinone fragment and aromatic/heterocyclic substituents at the C-11 position at  $\delta$  6.23–8.49 ppm is observed. The signal of the amide proton as a singlet appears at 10.80–12.58 ppm. The CH proton in the C-11 position occurred as singlet at 4.42–6.77 ppm, and the proton of the hydroxyl group of the naphthoquinone fragment in the C-9 position appeared as singlet between 10.31 and 11.76 ppm. The signal of the proton of the hydroxyl group of the naphthoquinone fragment in the C-9 position forms a singlet in the region of 10.31–11.76 ppm. In the  $^{13}\text{C}$  NMR spectra of the synthesized compounds, the signals observed at 166.9–185.3 were assigned to the carbonyl group (C=O) of the naphthoquinone moiety.

The regio-chemical assignment for compound **3.4** was confirmed by 2D NMR  $^1\text{H}$ – $^{13}\text{C}$  HMBC experiments. Thus, the key idea in elucidating the structure of compound **3.4** was to find the HMBC CH correlation of the proton of the tertiary carbon atom at 5.42 ppm and one of the doublets of the aromatic system ABC (7.31 and 7.56 ppm of the fragment “Ph-OH”) to characteristic carbons of keto groups with signals in a weak magnetic field (180.4 and 185.2 ppm). According to HMBC experiments, both protons at 5.42 and 7.56 ppm have HMBC correlations to different carbons of carbonyl groups in the values 185.2 and 180.4 ppm, respectively (**3.4**). In case of the existence of an alternative structure, the HMBC correlation of the above protons to the carbon of the carbonyl group (**3.4\***) would have to be observed, which, however, was absent (Fig. 3).

Structural features of synthesized compound **3.4** have been confirmed by single crystal X-ray diffraction study. As follows from the X-ray analysis, the investigated compound has the structure of 9-hydroxy-11-(4-methoxyphenyl)-3,11-dihydro-2H-benzo[6,7]thiochromeno[2,3-d]thiazole-2,5,10-trione and crystallizes as dimethylformamide solvate in a molar ratio of 1:1 (Fig. 3). The OH group present at the C-12 atom of the rigid tetracyclic 3,11-dihydro-2H-benzo[6,7]thiochromeno[2,3-d]thiazole-2,5,10-trione moiety forms an intramolecular hydrogen bond O20–H20...O21 (Fig. 4, Table 1), in which the O atom of the carbonyl group at position 14 acts as the proton acceptor.

The *p*-methoxyphenyl residue at the stereogenic C-16 atom occupies a pseudo-axial position, as can be seen from the angle of  $22.95(12)^\circ$  between C16–C22 bond vector and Cremer & Pople 4*H*-thiopyran ring plane normal [39]. Moreover, the phenyl ring of this residue forms a dihedral angle of  $89.87(6)^\circ$  with the mean plane of the slightly folded ( $\sigma$ . m.s.d. = 0.0967 Å) 4*H*-thiopyran system.

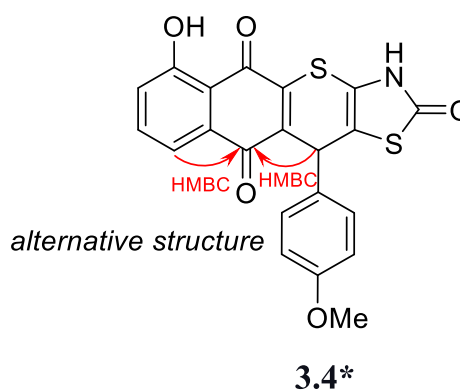
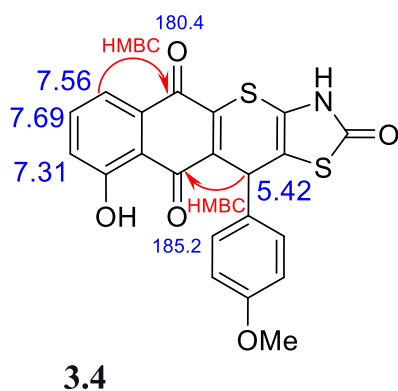


Fig. 3.  $^1\text{H}$  and  $^{13}\text{C}$  NMR chemical shifts of compound **3.4** with key interactions in the relevant HMBC spectra.

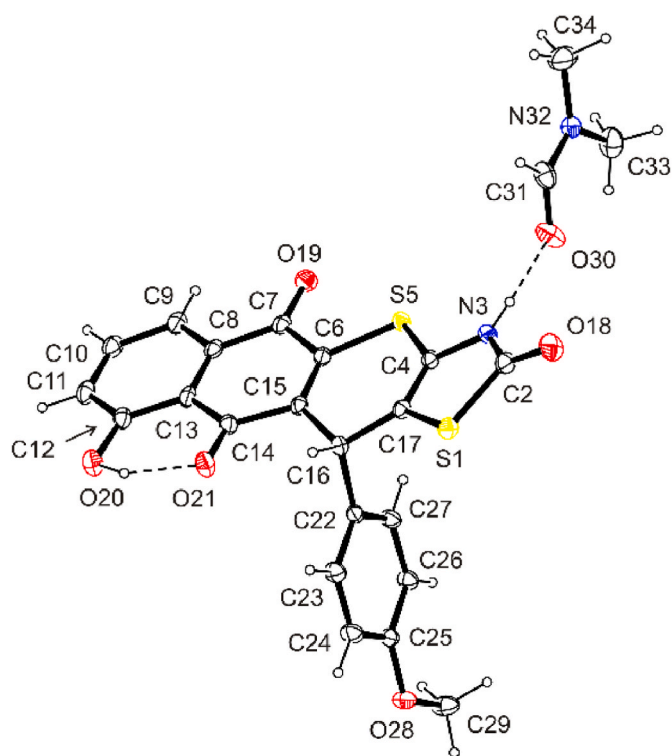


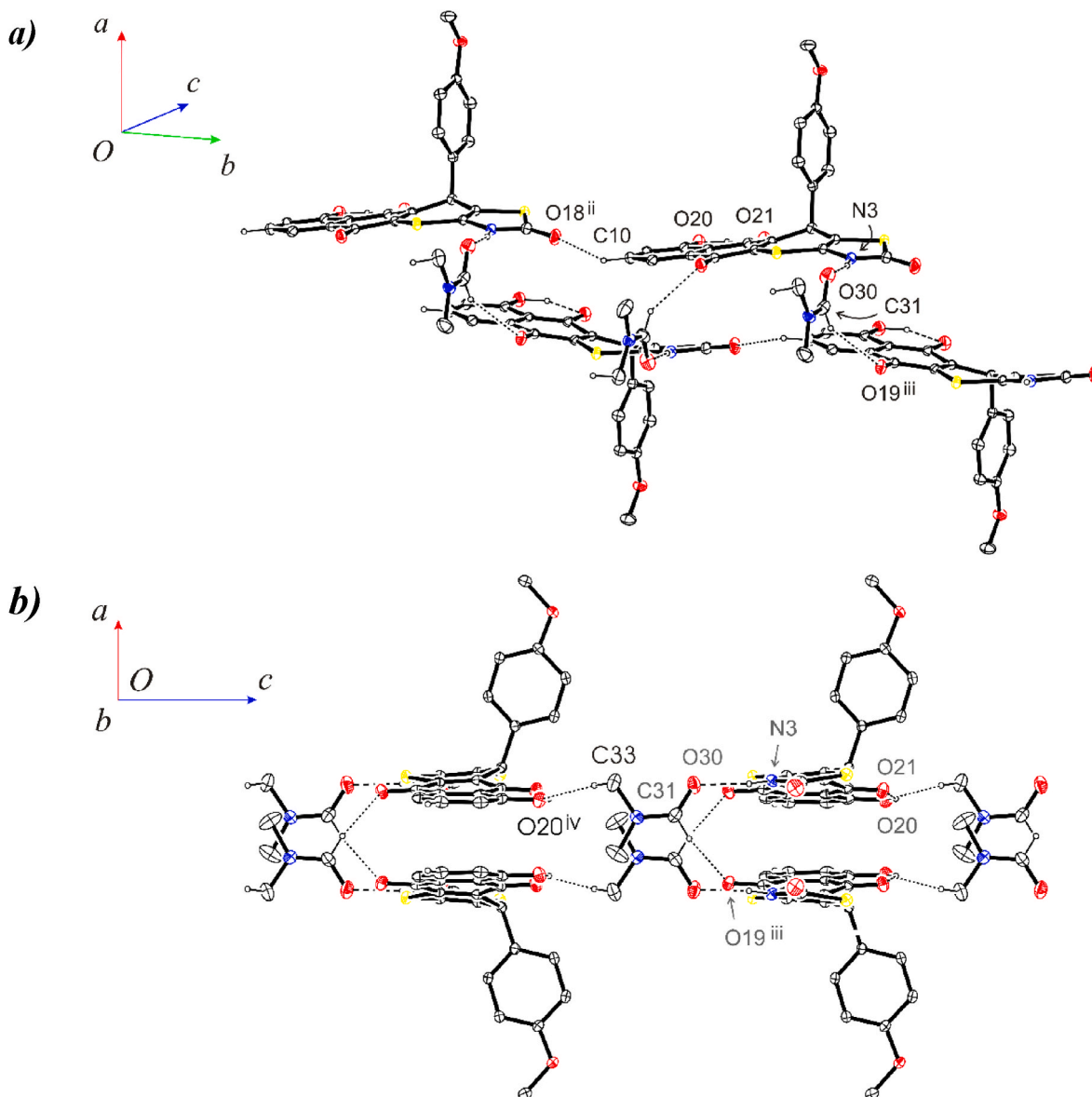
Fig. 4. ORTEP view of the molecule of **3.4\*DMF** showing the atomic labelling scheme. Non-H atoms are drawn as 30% probability displacement ellipsoids and H atoms are drawn as spheres of an arbitrary radius.

Table 1  
Hydrogen bonds and Y–X...Cg interactions in the crystal structure of **3.4\*DMF**.

D–H ... A	D–H (Å)	H ... A (Å)	D ... A (Å)	D–H ... A (°)
N3–H3...O30	0.85(3)	1.91(3)	2.736(3)	167(3)
O20–H20...O21	1.00(4)	1.74(4)	2.625(2)	145(3)
O20–H20...O28 <sup>i</sup>	1.00(4)	2.39(4)	2.948(2)	114(3)
C10–H10...O18 <sup>ii</sup>	0.95	2.38	3.082(3)	130
C31–H31...O19 <sup>iii</sup>	0.95	2.47	3.325(3)	149
C33–H33B...O20 <sup>iv</sup>	0.98	2.54	3.510(3)	172

Symmetry codes: (i)  $-1/2+x, 1/2-y, 1-z$ ; (ii)  $x, -1+y, z$ ; (iii)  $1/2-x, 1/2+y, z$ ; (iv)  $x, 1/2-y, -1/2+z$ .

Structural study has shown that the thiazolone system has the character of a  $\gamma$ -lactam. The position of the hydrogen atom bound to the N-3 atom was determined from the difference Fourier map and refined freely. Its presence in the mentioned position was confirmed by the hydrogen bond N3–H3...O30 (Fig. 5, Table 1), in which the carbonyl O-



**Fig. 5.** Hydrogen bonding in the crystal lattice of 3.4\*DMF: (a) hydrogen bonds N3-H3...O30, C10-H19...O18<sup>ii</sup> and C31-H31...O19<sup>iii</sup> linking the solvent molecules and the chains formed by solute molecules related by the glide plane *b*, (b) hydrogen bonds C33-H33B...O20<sup>iv</sup> linking adjacent antiparallel double chains into layers arranged parallel to the *bc* plane. The H atoms not involved in hydrogen bonds have been omitted for clarity.

30 atom of the solvent molecule acts as a proton acceptor. It was found that the interatomic distance C2-N3, 1.360(3) Å, in the thiazolone system is lengthened (by about 8σ) in relation to the literature bond length (O=C-NH, 1.331(2) Å [40]), for the secondary amide group of the γ-lactam system.

The observed interatomic distance C4-C17, 1.333(3) Å, confirms the occurrence of a double bond between the mentioned atoms {the reference C-C double bond length is 1.331(1) Å [40]}. In the crystal lattice, solute molecules related by translation along the *b*-axis are joined to each other by C10-H10...O18<sup>ii</sup> hydrogen bonds to form chains. The latter are further connected via solvent molecules (DMF) by hydrogen bonds N3-H3...O30, C31-H31...O19<sup>iii</sup> and C33-H33B...O20<sup>iv</sup> into layers growing parallel to the *bc* plane. Within the layer, solvent molecules connect with hydrogen bonds N3-H3...O30 and C31-H31...O19<sup>iii</sup> the adjacent chains related by the glide plane *b*, and further with hydrogen bonds C33-H33B...O20<sup>iv</sup> antiparallel pairs of chains (Fig. 2a and b, Table 1). The interpenetrating layers of molecules are further connected by hydrogen bonds O20-H20...O28<sup>i</sup> into a three-dimensional hydrogen bond network (Fig. 6, Table 1). It is worth noting that between the

thiazolone and benzene rings of the rigid quaternary 3,11-dihydro-2*H*-benzo[6,7]thiochromeno[2,3-*d*]thiazole-2,5,10-trione moieties of the molecules related by the glide plane *b* π...π contacts are also observed (Fig. 7). Perpendicular distances of Thi...Bz<sup>iii</sup> and Bz...Thi<sup>vi</sup> (-Thi = thiazol-2-one and Bz = benzene systems) amount to 3.4434(7) and 3.4345(8) Å, respectively.

### 2.1. *In vitro* evaluation of antitumor activity of newly synthesized thiopyranthiazoles

Some of synthesized compounds, namely 3.3, 3.9, and 3.10, were studied *in vitro* on 60 cancer cell lines representing nine different types (leukemia, melanoma, lung, colon, CNS, ovarian, renal, prostate, and breast cancers) at 10 μm concentration, according to the US NCI protocol (Table 2, Supplementary Figs. S27-S30), which was described previously [41-43]. The compounds were added at the mentioned concentration, and the cells were incubated for 48 h. The results for each compound are reported as the growth percent (GP%) of treated cells compared with untreated control cells. According to the results of



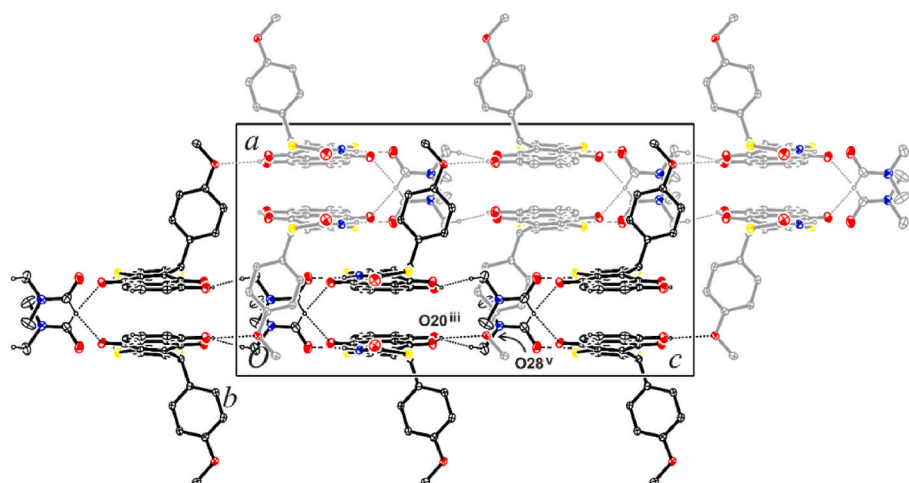


**Fig. 6.** Hydrogen bonding in the crystal lattice of 3.4\*DMF: interpenetrating layers of molecules connected by hydrogen bonds  $O20^{iii}-H20^{iii} \dots O28^v$ . For clarity, the H atoms not involved in hydrogen bonds have been omitted. Symmetry codes: (iii)  $1/2-x, 1/2+y, z$ , (v)  $1-x, 1-y, 1-z$ .

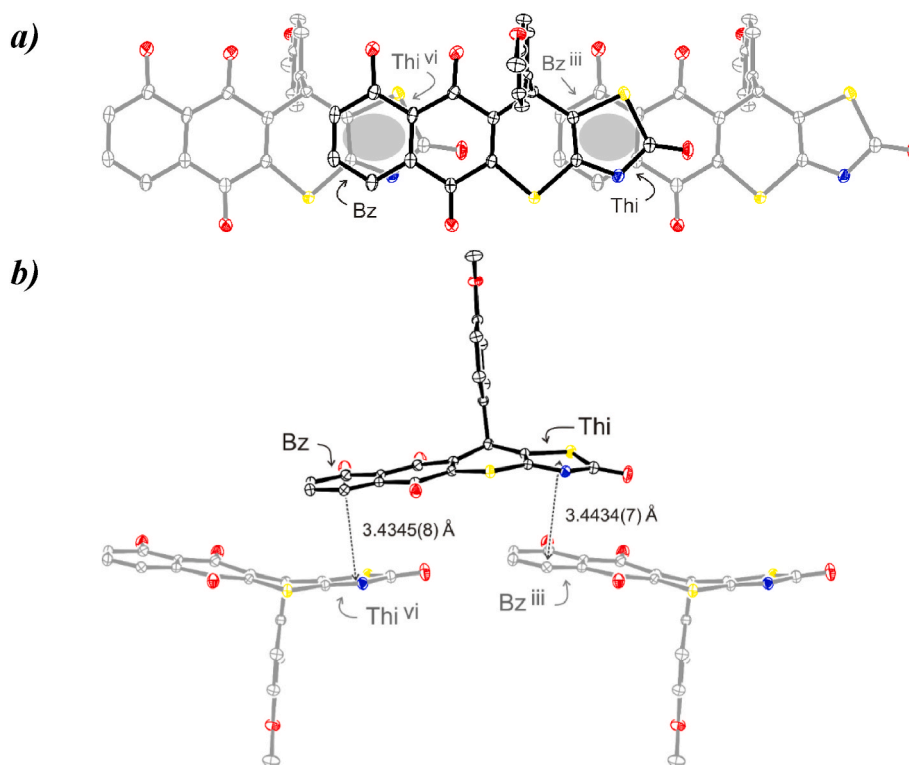


**Fig. 7.**  $\pi \cdots \pi$  Interactions between thiazol-2-one and benzene systems. Two projections of molecules showing (a) degree of  $\pi$ -rings overlap, and (b) inter-planar distances. For clarity, Hydrogen atoms have been omitted. Symmetry codes: (iii)  $1/2-x, 1/2+y, z$ , (vi)  $1/2-x, -1/2+y, z$ .

pre-screening, the two hit compounds, **3.9** and **3.10**, possessed prominent antitumor activity (mean growth  $-2.68\%$  (**3.9**);  $-61.06\%$  (**3.10**); the range of growth (**3.9**:  $-97.70$  to  $145.55\%$ ; **3.10**:  $-99.55$  to  $18.52$ ). In addition, they inhibited the growth of 48 (**3.9**) and 25 (**3.10**) tested cancer cell lines with percent growth of  $<0$ , and showed not only cytostatic effect but also cytotoxic properties.

In addition, compound **3.10** was selected in advanced assay for a panel of approximately sixty tumor cell lines at 10-fold dilutions of five concentrations (100  $\mu\text{M}$ , 10  $\mu\text{M}$ , 1  $\mu\text{M}$ , 0.1  $\mu\text{M}$  and 0.01  $\mu\text{M}$ ) [41–43]. The percentage of growth was evaluated spectrophotometrically after 48 h exposure using the sulforhodamine B (SRB) cytotoxicity assay of estimation of cell viability. Three antitumor activity dose-response parameters were calculated for each cell line:  $GI_{50}$  – molar concentration of

the compound that inhibits 50% net cell growth; TGI - molar concentration of the compound leading to the total inhibition; and  $LC_{50}$  - molar concentration of the compound leading to 50% net cell death (presented in negative logarithm). Furthermore, mean graph midpoints (MG\_MID) were calculated for each of the parameters, giving an average activity parameter over all cell lines for the tested compound. For the MG\_MID calculation, insensitive cell lines were included with the highest concentration tested. Compound **3.10** showed a broad spectrum of growth inhibition activity against tested human tumor cells with average  $GI_{50}$  and TGI values 2.91 and 14.70  $\mu\text{M}$ , respectively (Table 4, Supplementary Figs. S31–S33). The studied compound showed the highest efficiency against the melanoma line MALME-3M, with cytotoxicity at the sub-micromolar level (0.750  $\mu\text{M}$ ). The selectivity index (SI) obtained

**Table 2**  
Anticancer screening data of compound **3.3**, **3.9** and **3.10** at 10  $\mu\text{M}$  concentration.

Comp.NSC	Mean growth, %	Range of growth, %	Sensitive cell line growth, % (cancer line/type)	Positive cytostatic effect <sup>a</sup>	Positive cytotoxic effect <sup>b</sup>
<b>3.3</b> 839575	68.87	35.06 to 95.20	38.59 (SR/Leukemia) 35.06 (SF-539/CNS Cancer) 36.73 (CAKI-1/Renal Cancer) 39.78 (UO-31/Renal Cancer) 39.47 (BT-549/Breast Cancer)	8/58	0/58
<b>3.9</b> 839574	-61.06	-99.55 to 18.52	-94.27 (HOP-62/Non-Small Cell Lung Cancer) -96.80 (NCI-H322 M/Non-Small Cell Lung Cancer) -96.84 (HCC-2998/Colon Cancer) -91.39 (HCT-15/Colon Cancer) -93.51 (SF-295/CNS Cancer) -99.51 (SF-539/CNS Cancer) -99.55 (SNB-19/CNS Cancer) -99.39 (MALME-3M/Melanoma) -96.71 (M14/Melanoma) -90.20 (MDA-MB-435/Melanoma) -97.15 (SK-MEL-28/Melanoma) -96.94 (SK-MEL-5/Melanoma) -93.10 (UACC-257/Melanoma) -92.95 (OVCAR-5/Ovarian Cancer) -94.62 (OVCAR-8/Ovarian Cancer) -98.68 (A498/Renal Cancer) -97.36 (RXF 393/Renal Cancer) -92.79 (SN12C/Renal Cancer) -92.90 (UO-31/Renal Cancer) -99.86 (BT-549/Breast Cancer)	10/58	48/58
<b>3.10</b> 831848	-2.68	-97.70 to 145.55	-97.70 (NCI-H322 M/Non-Small Cell Lung Cancer) -92.30 (MALME-3M/Melanoma) -97.57 (M14/Melanoma) -93.38 (SK-MEL-5/Melanoma) -93.91 (DU-145/Prostate Cancer) -96.84 (BT-549/Breast Cancer)	25/57	25/57
<b>Doxo-rubicin</b> 759155	-20.30	-86.40 to 72.90	-81.60 (COLO-205/Colon Cancer) -76.10 (SNB-75/CNS Cancer) -71.60 (M14/ADR-RES/Melanoma) -82.60 (MDA-MB-435/Melanoma) -82.60 (SK-MEL-2/Melanoma) -86.40 (SK-MEL-5/Melanoma) -75.10 (A498/Renal Cancer)		

<sup>a</sup> Ratio between number of cell lines with percent growth from 0 to 50 and total number of cell lines.

<sup>b</sup> Ratio between number of cell lines with percent growth of <0 and total number of cell lines.

by dividing the full panel MG-MID ( $\mu\text{M}$ ) of the compound **3.10** by their individual subpanel MG-MID of cell line ( $\mu\text{M}$ ) was considered as a measure of compound's selectivity. In present study, the compound **3.10** was found to be nonselective at both the GI<sub>50</sub> and TGI doses (selectivity indexes 0.18–3.88 and 0.21–7.35, respectively) (Table 3).

According to the screening results, synthesized compounds were tested on their potential antitumor activity toward a panel of cancer cell lines including colon (HCT-116 wt, HCT-116 p53 (-/-), breast (MCF-7), leukemia (K562) and cervix (KB3-1). The compounds **3.1–3.4**, **3.7** and **3.10** demonstrated strongest cytotoxic effect toward all used tumor cell lines, and the IC<sub>50</sub> ranged from 0.6  $\mu\text{M}$  to 31.16  $\mu\text{M}$ . At the same time, a prominent activity of compounds **3.1**, **3.7** and **3.10** toward colon cancer cells (IC<sub>50</sub> was 0.75, 0.94 and 0.6  $\mu\text{M}$  respectively, Table 4) was depended on p53 status of cell line, wild type of HCT-116 cells was more sensitive to noted compounds compared with such p53-deficient cells. Derivatives **3.4** and **3.10** acted much more specifically towards KB3-1 cell line (IC<sub>50</sub> was 0.87 and 0.75  $\mu\text{M}$ , respectively). K562 cell line was sensitive to compounds **3.1**, **3.2**, **3.4** and **3.10**. MCF-7 cells were the most susceptible to the action of **3.7** (IC<sub>50</sub> was 0.95  $\mu\text{M}$ ). The compound **3.6** showed interesting selectivity toward this cell line, since only breast cancer cells were sensitive to its action. The compounds **3.5**, **3.9**, **3.11** showed moderate cytotoxic activity with the IC<sub>50</sub> from 4.53  $\mu\text{M}$  to 30.86  $\mu\text{M}$ , while the MCF-7 cells were the least sensitive to these derivatives, compared with other tumor cells. The **3.8**, **3.12** and **3.13** possessed low cytotoxic activity (IC<sub>50</sub> ranged from 9.48 to more than 50  $\mu\text{M}$ ). The juglone which was used for thiopyranothiazoles synthesis, showed a

weaker activity, compared with most active compounds **3.1**, **3.4**, **3.7** and **3.10**.

The harmful effect on human epidermal keratinocytes of HaCaT line, murine macrophages of J774.2 line and pseudonormal mouse fibroblasts of NIH 3T3 line also was studied. Cells of HaCaT line were insensitive to the action of synthesized thiopyranothiazoles **3.1–3.5**, **3.9**, **3.10** and **3.12** (IC<sub>50</sub> ranged from 37.16 to more than 50  $\mu\text{M}$ ). But for murine macrophages of J774.2 line and NIH 3T3 (normal mouse fibroblasts) these compounds were rather toxic, and the IC<sub>50</sub> ranged from 0.83  $\mu\text{M}$  to >50  $\mu\text{M}$ .

The compound **3.10** was investigated for its anti-leukemic activity towards the non-treated chronic lymphocytic leukemia (CLL), treated with bendamustine, and from donor with chronic lymphocytic leukemia recurrence after 4 years of remission, compared with the lymphocytes obtained from the peripheral blood of human donors (Table 5). The IC<sub>50</sub> was higher than 50  $\mu\text{M}$ , 8.24  $\mu\text{M}$ , and 28.18  $\mu\text{M}$ , respectively. The compound **3.10** showed the activity similar to doxorubicin's activity towards lymphocytes obtained from donor treated with the bendamustine, but other types of lymphocytes were resistant to its action. This thiopyrano[2,3-d]thiazole derivative was not toxic for the isolated lymphocytes from blood of healthy human donor (IC<sub>50</sub> > 50  $\mu\text{M}$ ).

Based on the obtained data, compound **3.10** demonstrated similar to doxorubicin, non-selective antineoplastic activity, but it was less toxic for pseudonormal cells (HaCaT, murine macrophages, mouse fibroblasts) and normal lymphocytes from healthy donor.

In addition to MTT assay, the biological efficiency of hit compound

**Table 3**  
Influence of compound **3.10** on growth of individual tumor cell lines.

	Cell line	GI <sub>50</sub> , μM	SI (GI <sub>50</sub> )	TGI, μM	SI (TGI)	LC <sub>50</sub> , μM	SI (LC <sub>50</sub> )
Leukemia	CCRF-CEM	3.29	0.88	>100.0	–	>100.0	–
	HL-60(TB)	1.82	1.59	6.09	2.41	>100.0	–
	K-562	2.84	1.02	>100.0	–	>100.0	–
	MOLT-4	2.71	1.07	9.88	1.48	>100.0	–
	RPMI-8226	2.62	1.11	9.83	1.49	>100.0	–
	SR	3.05	0.95	69.5	0.21	>100.0	–
	<b>MG_MID</b>	<b>2.72</b>	<b>1.06</b>	<b>49.21</b>	<b>0.29</b>	<b>&gt;100</b>	<b>–</b>
NSC lung cancer	A549/ATCC	1.78	1.63	3.63	4.04	7.38	6.17
	EKVX	6.75	0.43	19.4	0.75	44.3	1.02
	HOP-62	2.04	1.42	3.74	3.93	6.86	6.63
	HOP-92	3.15	0.92	8.08	1.81	32.5	1.40
	NCL-H266	2.18	1.33	5.46	2.69	27.3	1.66
	NCL-H322 M	1.71	1.70	3.13	4.69	5.74	7.93
	NCL-H460	1.54	1.31	3.48	4.22	7.84	5.80
	NCL-H522	2.31	1.25	6.99	2.10	26.4	1.74
	<b>MG_MID</b>	<b>2.68</b>	<b>1.08</b>	<b>6.73</b>	<b>2.18</b>	<b>19.79</b>	<b>2.30</b>
Colon cancer	COLO 205	1.89	1.53	3.61	4.07	6.93	6.57
	HCC-2998	2.50	1.16	5.51	2.66	18.4	2.47
	HCT-116	2.37	1.22	>100.0	–	>100.0	–
	HCT-15	1.75	1.66	3.88	3.78	8.59	5.30
	HT29	3.30	0.88	9.25	1.58	>100.0	–
	KM12	3.71	0.78	31.3	0.46	>100.0	–
	SW-620	3.28	0.88	10.5	1.4	52.7	0.86
	<b>MG_MID</b>	<b>2.68</b>	<b>1.08</b>	<b>23.43</b>	<b>0.62</b>	<b>55.23</b>	<b>0.82</b>
	CNS cancer	SF-268	3.48	0.83	19.2	0.76	>100.0
SF-295		1.98	1.46	3.59	4.09	6.50	7.00
SF-539		1.93	1.50	3.69	3.98	7.05	6.46
SNB-19		2.60	1.11	7.33	2.00	26.1	1.74
SNB-75		3.17	0.91	7.61	1.93	25.8	1.76
U251		3.07	0.94	10.1	1.45	35.7	1.27
<b>MG_MID</b>		<b>2.70</b>	<b>1.07</b>	<b>8.58</b>	<b>1.71</b>	<b>33.52</b>	<b>1.35</b>
Melano-ma	LOX IMVI	2.21	1.31	7.55	1.94	84.0	0.54
	MALME-3M	0.75	3.88	2.00	7.35	4.75	9.58
	M14	1.06	2.74	2.37	6.20	5.26	8.65
	MDA-MB-435	1.16	2.50	2.47	5.95	5.26	8.65
	SK-MEL-2	3.51	0.82	16.4	0.89	52.9	0.86
	SK-MEL-28	1.87	1.55	3.72	3.95	7.42	5.90
	SK-MEL-5	1.59	1.83	3.00	4.90	5.68	8.01
	UACC-257	1.57	1.85	3.26	4.50	6.75	6.78
	UACC-62	1.76	1.65	3.43	4.28	–	–
	<b>MG_MID</b>	<b>1.72</b>	<b>1.69</b>	<b>4.91</b>	<b>2.99</b>	<b>19.11</b>	<b>2.38</b>
Ovarian cancer	IGROV1	2.51	1.15	6.14	2.39	38.0	1.19
	OVCAR-3	2.86	1.01	14.0	1.05	>100.0	–
	OVCAR-4	1.79	1.62	3.95	3.72	8.71	5.22
	OVCAR-5	2.13	1.36	4.58	3.20	9.85	4.62
	OVCAR-8	2.46	1.18	8.97	1.63	36.2	1.25
	NCI/ADR-RES	3.02	0.96	12.3	1.19	>100.0	–
	SK-OV-3	15.5	0.18	29.6	0.49	56.5	0.80
	<b>MG_MID</b>	<b>4.32</b>	<b>0.67</b>	<b>11.36</b>	<b>1.29</b>	<b>49.89</b>	<b>0.91</b>
Renal Cancer	786-0	7.09	0.41	24.2	0.60	71.2	0.63
	A498	3.48	0.83	9.69	1.51	31.6	1.44
	ACHN	4.08	0.71	16.1	0.91	40.1	1.13
	CAKI-1	3.29	0.88	13.9	1.05	37.3	1.22
	RXF 393	2.02	1.44	5.57	2.63	20.1	2.26
	SN12C	1.74	1.67	3.49	4.21	6.99	6.51
	TK-10	12.3	0.23	26.4	0.55	56.4	0.80
	UO-31	2.56	1.13	13.5	1.08	36.7	1.24
	<b>MG_MID</b>	<b>4.57</b>	<b>0.63</b>	<b>14.10</b>	<b>1.04</b>	<b>37.54</b>	<b>1.21</b>
	Prostate Cancer	PC-3	2.75	1.05	21.6	0.68	>100.0
DU-145		1.55	1.87	3.01	4.88	5.81	7.83
<b>MG_MID</b>		<b>2.15</b>	<b>1.35</b>	<b>12.30</b>	<b>1.19</b>	<b>52.90</b>	<b>0.86</b>
Breast cancer	MCF7	1.39	2.09	3.34	4.40	8.04	5.66
	MDA-MB-231/ATCC	2.73	1.06	9.08	1.61	>100.0	–
	HS 578T	2.20	1.32	6.56	2.24	>100.0	–
	BT-549	1.64	1.77	3.19	4.60	6.22	7.32
	T-47D	2.87	1.01	13.0	1.13	>100.0	–
	MDA-MB-468	2.01	1.44	6.59	2.23	>100.0	–
<b>MG_MID</b>	<b>2.14</b>	<b>1.35</b>	<b>6.96</b>	<b>2.11</b>	<b>69.04</b>	<b>0.65</b>	
<b>MG_MID</b>	<b>2.91</b>		<b>14.70</b>		<b>45.55</b>		



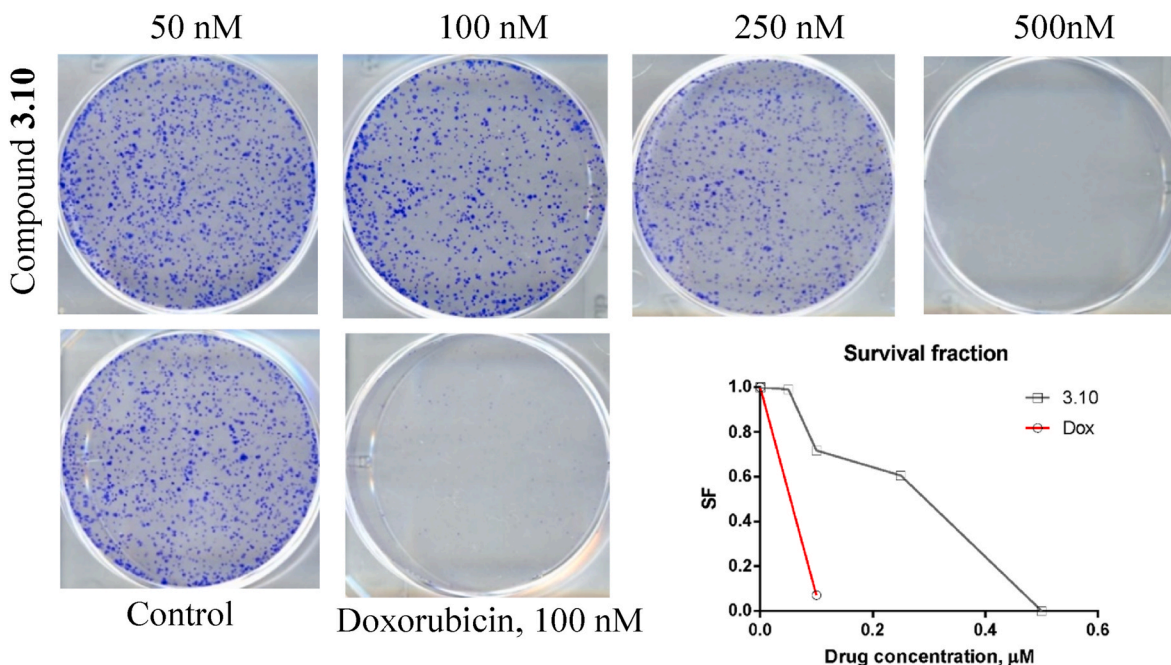
**Table 4**IC<sub>50</sub> of studied compounds (MTT test, 72 h of treatment, M ± SD, n/d - not determined).

Comp./Cell Line	HCT-116	HCT-116 p53 (-/-)	MCF-7	KB3-1	K562	J774.2	NIH 3T3	HaCaT
<b>3.1</b>	0.75± 0.35	3.86± 0.32	9.34± 0.12	3.64± 0.43	11.83± 0.38	5.25± 0.67	36.95± 0.87	>50
<b>3.2</b>	4.70± 0.22	3.82± 0.19	31.16± 0.32	2.74± 0.18	6.31± 0.11	2.03± 0.41	30.44± 0.45	>50
<b>3.3</b>	4.12± 0.11	3.10± 0.41	7.50± 0.56	3.33± 0.21	19.22± 0.22	5.27± 0.23	46.63± 0.13	>50
<b>3.4</b>	3.19± 0.13	3.26± 0.90	6.10± 0.21	0.87± 0.11	5.66± 0.31	2.95± 0.25	6.78± 0.34	40.84± 0.44
<b>3.5</b>	6.15± 0.33	8.83± 0.25	>50	7.21± 0.41	22.90± 0.18	26.89± 0.98	>50	>50
<b>3.6</b>	35.60± 0.21	43.70± 0.41	7.41± 0.41	46.38± 1.09	28.38± 0.87	7.44± 0.11	n/d	n/d
<b>3.7</b>	0.94± 0.11	2.16± 0.43	0.95± 0.10	6.94± 0.18	15.68± 0.56	0.83± 0.45	n/d	n/d
<b>3.8</b>	40.63± 0.13	41.69± 0.55	>50	47.53± 0.30	33.00± 0.54	30.83± 0.65	n/d	n/d
<b>3.9</b>	5.13± 0.22	5.36± 0.98	24.08± 0.13	4.53± 0.31	21.52± 0.48	6.81± 0.34	39.08± 0.95	>50
<b>3.10</b>	0.6± 0.24	2.37± 0.43	3.08 ± 0.41	0.75± 0.29	5.98± 0.41	2.59± 0.13	6.07± 0.41	37.16± 0.56
<b>3.11</b>	5.44± 0.80	6.28± 0.87	29.02± 0.20	5.54± 0.35	30.86± 0.22	6.77± 0.25	38.89± 0.88	n/a
<b>3.12</b>	12.9± 0.11	36.20± 0.21	9.48± 0.11	23.38± 0.98	26.80± 0.45	26.39± 0.38	>50	>50
<b>3.13</b>	>50	>50	>50	>50	>50	>50	n/d	n/d
<b>Juglone</b>	31,6	n/d	n/d	26,4	n/d	13,36	n/d	n/d
<b>Doxoru-bicin</b>	0.58± 0.10	0.63± 0.08	0.62± 0.13	0.56± 0.25	0.59± 0.11	0.72± 0.98	4.56± 1.00	0.78

**Table 5**IC<sub>50</sub> of compound **3.10** (MTT test, 72 h of incubation, M ± SD).

Comp./Cell Line	CLL non-treated	CLL treated	CLL remission	Lymphocytes of healthy donor
<b>3.10</b>	>50	8.24 ± 0.32	28.18 ± 0.68	>50
<b>Dox</b>	>10	8.60 ± 0.98	7.33 ± 1.03	10.00 ± 2.01

**3.10** was determined using the clonogenic assay. It was found that survival fraction of the cells after drug expose with the **3.10** was almost 14 times bigger comparing to survival fraction after incubation of KB-3-1 cells with doxorubicin in the same concentration (100 nM) used as a positive control. However, at applying 500 nM concentration of the compound **3.10**, we did not observe the growth of KB-3-1 cell colonies after 72 h of drug exposure (Fig. 8).

**Fig. 8.** Representative cell culture wells and graphical data of the result of colony test performed on KB-3-1 cells.

## 2.2. COMPARE analysis and molecular docking simulations

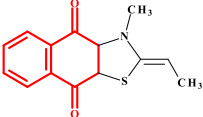
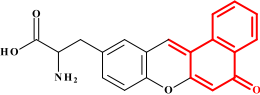
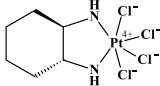
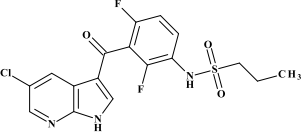
Compare analysis and docking simulation for the **3.10** were performed to gain a comprehensive understanding of plausible modes of action and the quantitative expression of the anticancer activity, compared to standard therapeutic agents (Table 6). For comparing the sets, neither marketed drugs nor standard agents yielded sufficient results. The highest Pearson coefficient was 0.54, which is not statistically proven [44]. Nevertheless, using the Synthetic compounds dataset for calculation gained the result of 0.75 with the compound NSC695501. Pubchem portal (<https://pubchem.ncbi.nlm.nih.gov/>) mentions the results of the different biological assays, where NSC695501 was confirmed as modulator of Transforming growth factor  $\beta$  (TGF- $\beta$ ) signaling pathway (BioAssay AIDs 588855, 720534 and 588856) with IC<sub>50</sub> range from 1.4125  $\mu$ M to 2.2387  $\mu$ M.

According to the results of COMPARE analysis, the structure of the TGF $\beta$  was used as a target for further docking simulation. In addition, we included the topoisomerase I, II and human dihydroorotate dehydrogenase (hDHODH), owing to literally reported ligands with 1,4-benzoquinone scaffold for those proteins [45,46]. Docking scores are listed in Table 7.

Docking scores confirmed the possible mode of action through the TGF $\beta$  inhibitions (Fig. 9). The binding energy of the **3.10** with TGF $\beta$  is close to the reference ligand CID 5287512. **3.10** did not show any significant affinity to both Topoisomerases, compared to its standard inhibitors, nevertheless structure's resemblance with the doxorubicin.

High affinity of the **3.10** to TGF $\beta$  are achieved owing to four hydrogen bonds with ASP351 (2.07 Å), LYS337 (2.67 Å), LYS332 (2.01 Å) and ALA230 (2.92 Å). Also, ALA350, VAL219, LEU260 and LEU360 form different types of the hydrophobic interactions (Pi-Sigma, Pi Alkyl, Pi-Cation) with lipophilic amino acids inside the binding site. Compared to the native 1,5-naphthyridine derivative ligand **3.10** forms more hydrogen bonds inside ATP binding pocket (4 bonds vs 3 bond), however there is no interaction with HIS283. Nevertheless, the **3.10** interplays with the flexible ASP351, and as was suggested by Sawyer et al. the interaction with ASP351 side chain might play a key role in the

**Table 6**  
COMPARE analysis of compounds **3.10** with different sets (at GI<sub>50</sub> values).

Compound	PCC	Dataset	Mechanism of action
NSC695501	0.75	Synthetic compounds	TGF $\beta$ inhibitor
			
NSC643735	0.64	Diversity set	Unknown
			
NSC363812	0.54	Standard agents	Binding to DNA
			
NSC761431 Vemurafenib	0.42	Marketed drugs	inhibitor of BRAF kinase
			

PCC – Pearson correlation coefficient and PCC values > 0.6 are considered to indicate a significant similarity to tentatively tested anticancer agents.

ability of TGF $\beta$  to accumulate a range of inhibitors [47]. Additional stabilization of the complex is supported by carbon hydrogen bonds with the ASP281 and SER287 (Fig. 10).

TGF- $\beta$  is a very interesting target for anticancer agents. Besides, TGF- $\beta$  is a unique cytokine since for cells of epithelial tissues, including the malignant ones, it is a powerful inhibitor of growth and an inducer of apoptosis. Its action towards tumor cell strongly depends on the transformation status of the target cells. TGF $\beta$ 1 inhibited proliferation of normal cells or weakly transformed tumor cells. However, it did not inhibit proliferation of highly transformed malignant cells, while activating migration of these cells causing a development of metastasis [48].

## 2.3. Reactivity with reduced glutathione (GSH)

The reactivity of the un-metabolized juglone, **2.10**, and the compound **3.10** was assessed in the test with the model soft nucleophile reduced glutathione (GSH) (Fig. 11). It has been found that after the incubation with these compounds, the level of GSH decreases and does not increase significantly with adding of sodium borohydride, which suggests the formation of covalent GS-adducts that are not reduced to GSH with sodium borohydride, unlike the oxidized glutathione GSSG.

## 2.4. Interaction of synthesized compounds with DNA

Next, we investigated DNA-binding ability of the tested compounds using Methyl Green (MG) test, KMnO<sub>4</sub> DNA oxidation reaction and UV-Visible spectroscopy. The importance of DNA-binding agents cannot be overstated, as many anticancer therapies include drugs that bind and/or modify DNA [49]. The main advantage of such compounds is their selectivity for tumor cells with defects in the DNA repair [50].

The MG displacement test is a useful biochemical screen for the detection of biologically active compounds that interact with DNA. All derivatives under study showed a certain capacity of interacting with DNA. Compounds **3.5**, **3.7**, **3.9**, **3.10** and **3.12** replaced MG to the greatest extent, the percentage of MG replacement was 55.4, 53.2, 66.4, 44.3 and 42.5, respectively, and approached that of juglone and doxorubicin (55.4, 65.3 and 72.3%). The **3.1–3.4**, and **3.8** showed middle capacity to MG replacement, from 29.5 to 37.35%. Other derivatives such as **3.6**, **3.11**, and **3.13** replaced MG to the smallest extent, % of replacement ranged from 11.8 to 20.7% (Fig. 12).

The interaction of the derivatives suggested their ability to arrest DNA synthesis in cell lines under investigation in the order **3.9** > **3.5** > **3.7** > **3.10** > **3.12** > **3.2** > **3.4** > **3.3** > **3.8** > **3.1** > **3.11** > **3.13** > **3.6**. This order does not correlate with the result of MTT test, however, two of the most active compounds **3.7**, and **3.10** interact with DNA to a large extent. These results may indicate that more active compounds have other mechanisms of action, besides DNA interaction.

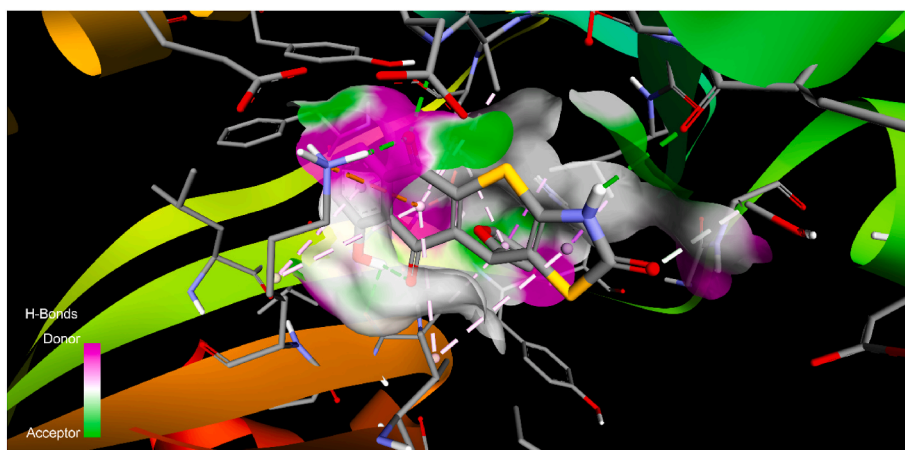
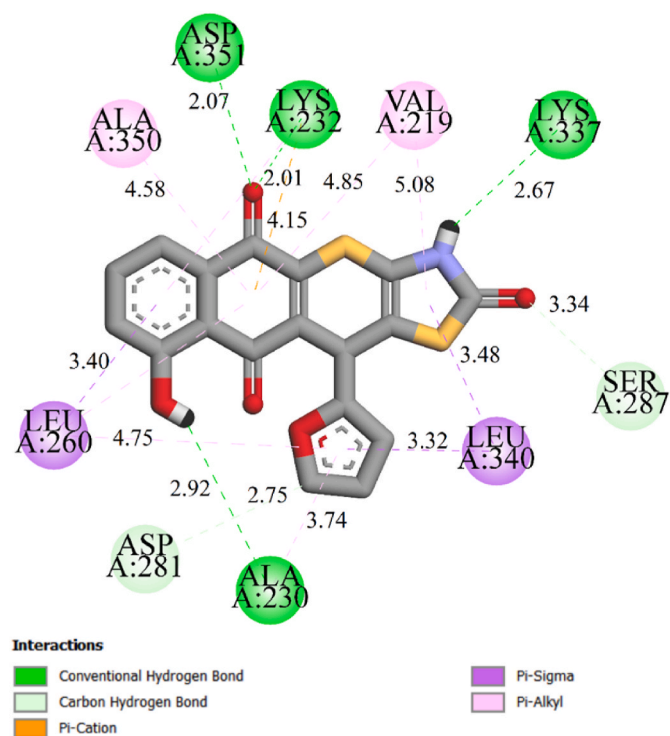
The KMnO<sub>4</sub> oxidation reaction was used to study the selective oxidation of pyrimidine bases, particularly thymidine, in regions of DNA damage by the most active derivative **3.10**. Compounds that interact with DNA distort its duplex structure, thus, subjecting pyrimidine bases to KMnO<sub>4</sub> oxidation, the formed products can be detected using UV/VIS spectrophotometry. This assay allows to detect different classes of DNA binding agents [51]. The results of these studies showed that the level of permanganate oxidation of salmon sperm DNA induced by compound **3.10** demonstrated a similar dose-dependent tendency with **2.10** (Fig. S35). NetAbs for reaction with dsDNA was from -0.836 to 0.562 for **3.10**, and from -0.259 to 0.637 – for **2.10**. The juglone showed time-dependent effect, NetAbs was from -0.030 to 0.490.

In addition, the measurement of UV-Visible absorption spectra of compound **3.10** and its complex with DNA was used for a more detailed study of the possible type of interaction with DNA. Any change in the conformation and structure of DNA that occurs on binding of small molecule translates into a change in its spectral behavior. Hypochromic effect occurs when a molecule binds to DNA and stabilize its structure and hyperchromism occurs as a result of the destruction of the secondary

Table 7

Binding energy values obtained during docking analysis of complex TGF $\beta$ , Topoisomerase I, Topoisomerase II and hDHODH with **3.10**.

Docked ligands	TGF $\beta$ (PDB 1VJY)		Topoisomerase I (PDB 1T8I)		Topoisomerase II (PDB 3QX3)		hDHODH (PDB 6LP7)	
	Binding energy	Ki, $\mu$ M	Binding energy	Ki, $\mu$ M	Binding energy	Ki, $\mu$ M	Binding energy	Ki, $\mu$ M
<b>3.10</b>	-8.91	0.293	-7.33	4.24	-8.44	0.652	-8.20	0.976
CID 5287512	-9.69	0.078	-	-	-	-	-	-
Etoposide	-	-	-	-	-13.05	0.0003	-	-
Doxorubicin	-8.33	0.784	-9.25	0.165	-12.03	0.0015	-5.06	195.31
Camptothecin	-	-	-10.42	0.023	-	-	-	-
CID 154700495	-	-	-	-	-	-	-11.94	0.0017

Fig. 9. Predicted binding mode of **3.10** at the binding site of crystal structure of TGF $\beta$  (PDB 1VJY).Fig. 10. 2D scheme of the TGF $\beta$ -**3.10** complex.

structure of DNA. Absorption spectrum of the **3.10** exhibited bands at 262, 362, and 420 nm (Fig. 13). With the addition of increasing amounts of DNA, the absorbance of the **3.10** increased at 262 nm, while those at 362 and 420 nm decreased slightly. The hyperchromic effect, observed at 262 nm, and blue shift is the result of destabilization of the secondary

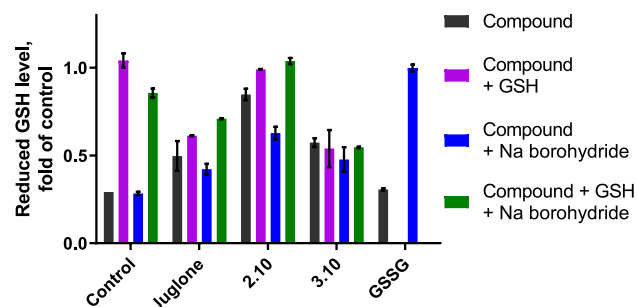


Fig. 11. The results of measuring the reduced glutathione (GSH) level.

structure of DNA by small molecules. Such effect can be observed due to the occurrence of electrostatic interaction between DNA and the compound. The formation of isosbestic point at around 300 nm in combination the slight hypochromism observed at 362, and 420 nm is associated with the formation of the new **3.10**-DNA complex and intercalation of the **3.10** into DNA base pairs [52]. Thus, this compound is capable of interacting with DNA in two ways.

### 2.5. Apoptosis induction in KB3-1 cells

We used fluorescent microscopy of cells stained with Hoechst-33342, DNA laddering assay, Western-blot assays, and FACS analysis in order to estimate the potential pro-apoptotic pathways affected by derivative **3.10** in the treated cells.

The Hoechst-33342 stain was used to qualitatively evaluate whether the compound **3.10** mediated toxic effects on KB3-1 cells were due to the activation of apoptotic pathways. Treatment of KB3-1 cells with the **3.10** resulted in cytomorphological changes. The condensed chromatin and

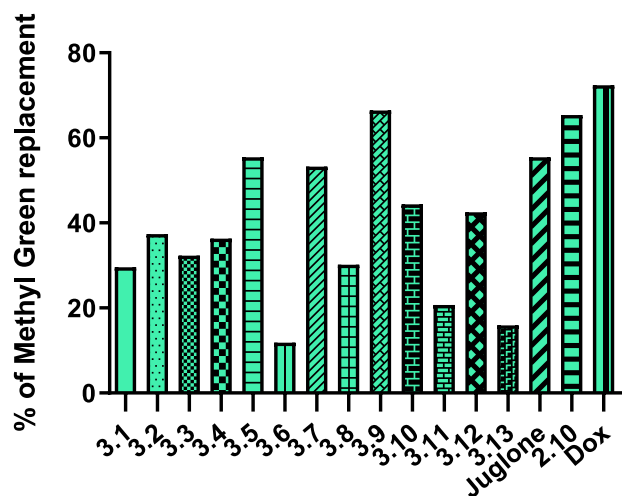


Fig. 12. Replacement of methyl green in salmon sperm DNA by the synthesized compounds 3.1–3.13, Juglone, 2.10, and doxorubicin used in 10  $\mu\text{M}/\text{mL}$  concentration.

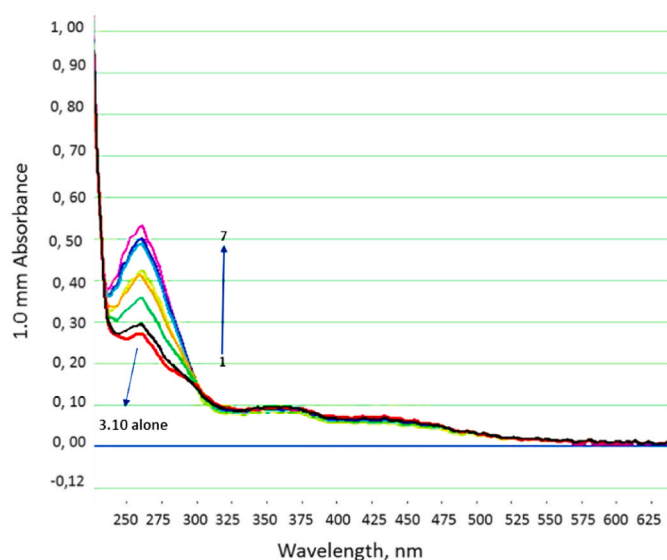


Fig. 13. UV–Visible absorption spectra of 250  $\mu\text{M}/\text{mL}$  of compound 3.10 in presence of different concentrations of DNA 20 (1, black line), 40 (2, green line), 60 (3, orange line), 80 (4, light green line), 100 (5, light blue line), 120 (6, blue line), and 140 (7, pink line)  $\mu\text{g}/\text{mL}$ .

membrane blabbing (Supplementary Fig. S34B) could be found under the 3.10 effect in comparison with untreated (control) cells (Supplementary Fig. S34A). Doxorubicin induced similar changes (chromatin condensation and membrane blabbing) in treated KB3-1 cells (Supplementary Fig. S34C). One can assume that compound 3.10 caused the pro-apoptotic cytomorphological changes in KB3-1 cells. The compound 3.10 demonstrated red fluorescence (Red channel, Supplementary Fig. S34B) in the treated cells, similar to doxorubicin (Supplementary Fig. S34C).

Apoptosis-inducing potential of compound 3.10 was confirmed by DNA laddering assay. DNA fragmentation is the known marker of apoptosis process which activates the caspase-3 [53]. The result, presented in the Supplementary Fig. S36 (lines 2, 3, 4, 5) shows that the process of apoptosis was initiated by compound 3.10, by causing damage of DNA in Jurkat cells. In the concentration of 25  $\mu\text{M}$

(Supplementary Fig. S36, line 6) 3.10 induced more necrotic degradation of DNA. Doxorubicin at 1  $\mu\text{M}$ , which was used as the positive control, at 0.5  $\mu\text{M}$  induced necrotic changes in treated Jurkat cells.

## 2.6. Effect of 3.10 on cell cycling

Cell cycle dysregulation is a distinguishing feature of the conversion of normal cells into malignant cells. Due to the role that the cell cycle plays in carcinogenesis, a number of cell cycle inhibitors have gained attention as potential therapeutic medications for the treatment of cancer, both on their own and in combination with conventional cytotoxic or molecular targeting therapies [54].

CCRF-CEM leukemia cells were used as a model cell line to investigate the effect of 3.10 on the cell cycle. These cells were sensitive to 3.10 with an  $\text{IC}_{50}$  of  $4.14 \pm 0.32 \mu\text{M}$ . Compound 3.10 increased the percentage of cells in the sub-G1 phase of the cell cycle in  $1 \times \text{IC}_{50}$  and, as expected, even more at  $5 \times \text{IC}_{50}$  (Table 8). The sub-G1 peak is made up of apoptotic cells and also cells that have already lost their DNA by releasing apoptotic bodies, cell fragments with chromatin fragments, damaged nuclei, chromosomes and cellular detritus [55]. The 3.10 showed the tendency to diminish the proportion of cells in the G0/G1 phase and increase the proportion of cells in the G2/M phase compared to the control. The 3.10 decreased the proportion of cells actively synthesizing DNA and RNA.

## 2.7. Effect of the compound 3.10 on stress of endoplasmic reticulum

It was shown that the juglone, which is a component of the compound 3.10, can use the stress of endoplasmic reticulum (ER) for induction of apoptosis [33]. That is why the next step of our work was to check changes in the amount of proteins involved in the stress of ER. To do that, we used Western-blot analysis of BIP (immunoglobulin heavy chain binding protein), PDI (oxidoreductase protein-disulfide isomerase) and Calnexin in the lysates of KB-3-1 cells depending on time (3 h and 24 h) and dose (0.5, 2.5 and 5  $\mu\text{M}$ ) of the 3.10 used for cell treatment. We did not find changes in the level of abovementioned proteins at 3 h term of the compound action. However, at 24 h term, a dose-dependent increase in BIP level was detected (Fig. 14). BIP is a HSP70 molecular chaperone located in the lumen of the ER. It binds newly synthesized proteins when they are translocated into the ER, and maintains them in a state competent for subsequent folding and oligomerization. As a UPR (unfolded protein response) target gene product, BIP is upregulated when UPR transcription factors associate with the UPR element in BIP's DNA promoter region [56]. The UPR is activated in response to an accumulation of unfolded or misfolded proteins in the lumen of the endoplasmic reticulum. In this scenario, the UPR has three aims: initially to restore normal function of the cell by halting protein translation, degrading misfolded proteins, and activating the signaling pathways that lead to increasing the production of molecular chaperones involved in protein folding. If these objectives are not achieved within a certain time span or the disruption is prolonged, the UPR aims towards apoptosis [57].

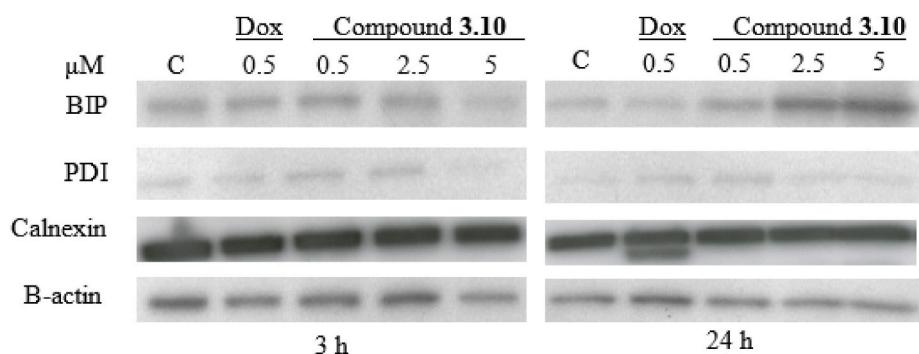
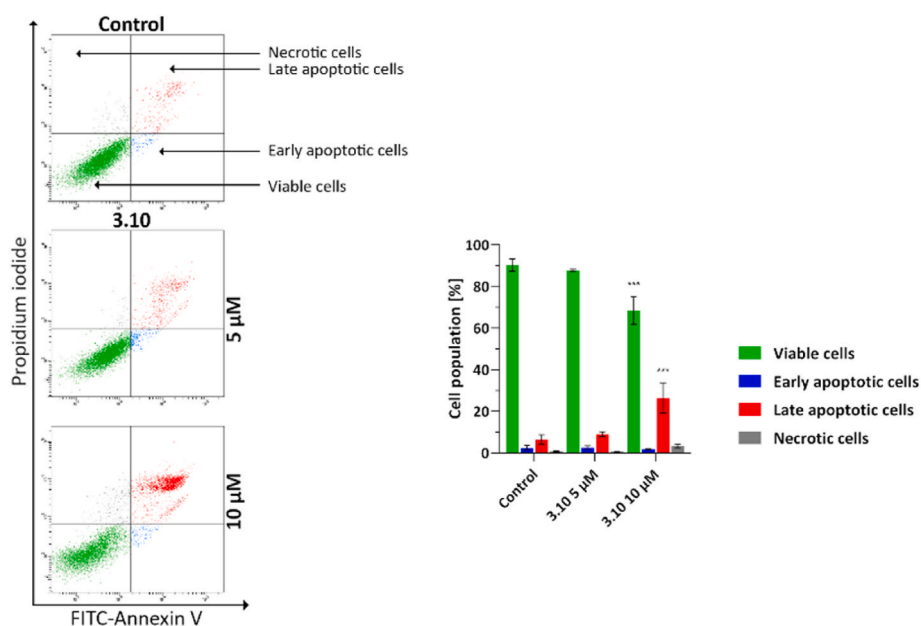
## 2.8. Induction of apoptosis by decreasing mitochondrial membrane potential by compound 3.10

For quantitative determination of the apoptotic effects of compound 3.10 in MDA-MB-231 cells, flow cytometric assay was performed using double staining Annexin V-FITC and Propidium iodide (AV/PI). This study allowed for differentiation of four cell populations: cells not stained (alive cells), cells stained with Propidium iodide (necrotic cells), cells stained with FITC-labeled Annexin V (early apoptotic cells) and cells stained with Annexin V and Propidium iodide (late apoptotic cells). In case of applying the 3.10, 11.7% (5  $\mu\text{M}$ ) and 28.2% (10  $\mu\text{M}$ ) of apoptotic cells were detected. In control, the amount of apoptotic cells was 8.9% (Fig. 15).



**Table 8**The effect of **3.10** on the cell cycle (G0/G1, S, G2/M), apoptosis (sub-G1), M phase (+pH3<sup>Ser10<sup>a</sup></sup>), DNA and RNA synthesis analysis in CCRF-CEM cells.

Tested concentration	Sub-G1 (apopto-sis)	G0/G1	S	G2/M	>G2/M	M	DNA synthesis	RNA synthesis
Control	2.36± 0.049	38.68±	41.09±	20.24±	10.09±	1.97±	42.40±	31.80±
1 × IC <sub>50</sub> (4.14 μM)	5.02	34.34	41.83	23.82	12.23	1.25	19.29	23.46
5 × IC <sub>50</sub> (20.7 μM)	5.80	35.58	42.33	22.09	20.54	1.70	0.90	0.07

<sup>a</sup> Phospho-Histone H3 (Ser10).**Fig. 14.** Results of electrophoretic study (Western blot analysis) of proteins of ER stress response in cell lysates of KB-3-1 cells treated for 3 and 24 h with the compound **3.10** applied in different concentrations. Doxorubicin was used as positive control.**Fig. 15.** Results of flow cytometry analysis of MDA-MB-231 breast cancer cells after 24 h incubation with **3.10** (concentration 5 μM and 10 μM) and subsequent staining of cells with Annexin V and propidium iodide. The obtained results are presented as mean values ± SD obtained from three independent experiments (n = 3) done in duplicate. \*p < 0.05 vs. control group, \*\*\*p < 0.001 vs. control group.

Apoptosis may proceed in the treated cells via two pathways - extrinsic (cell death receptor-mediated) and intrinsic (mitochondria-mediated). In the extrinsic pathway, after stimulation of death receptors, recruitment of adaptor molecules, formation of death-inducing signaling complex (DISC), and then, activation of caspase 8 and 10 occurs. This, along with the subsequent activation of executory caspases, leads to cell death [58]. Considering the important role of caspase 8 in the initiation of apoptosis via the extrinsic pathway, we evaluated the effects of the compound **3.10** on the activation of this protein in MDA-MB-231 breast cancer cells after 24 h exposure (concentrations of 5 and 10 μM). It was found that the tested compound increased the amount of active form of this caspase (Fig. 16). There was 19.5% of cells with active caspase 8 at

treatment with **3.10** at 5 μM and 62.7% - at 10 μM of the tested compound. The results of evaluating caspase 8 activities are consistent with those obtained in the AV/PI assay, indicating that apoptosis induced by the tested compound may proceed via an extrinsic pathway mediated by cell death receptors.

Triggering factors for the intrinsic pathways of apoptosis with mitochondria involvement also include DNA damage or oxidative stress [59]. We investigated the effect of the tested compound **3.1** on the mitochondrial membrane potential ( $\Delta\Psi_m$ ) in MDA-MB-231 cells treated for 24 h in concentrations (5 μM and 10 μM). To do that, cytometric analysis using JC-1 dye was applied. JC-1 is a carbocyanine lipophilic cationic fluorochrome that can take on different forms and fluorescence

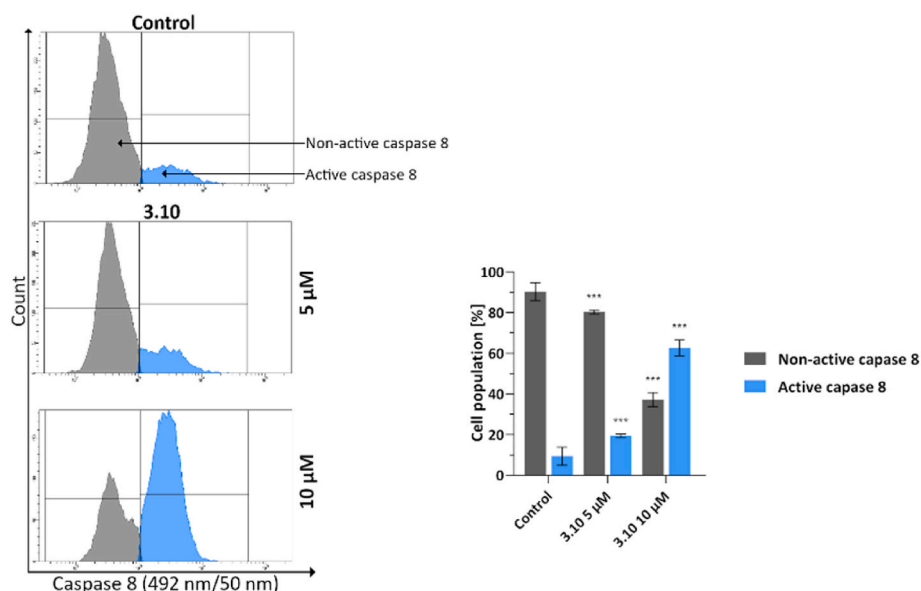


**Fig. 16.** The results of flow cytometry measurement analysis of caspase 8 activity in the MDA-MB-231 breast cancer cells after their 24 h treatment incubation with **3.10** (concentration 5  $\mu$ M and 10  $\mu$ M). The obtained results are presented as mean values  $\pm$  SD obtained from three independent experiments ( $n = 3$ ) done in duplicate. \*\*\* $p < 0.001$  vs. control group.

depending on the MMP. In viable cells with normally functioning mitochondria, this dye accumulates in the hyperpolarized mitochondrial membrane to form aggregates that emit red fluorescence. While in apoptotic or necrotic cells, these aggregates disintegrate and monomers with green fluorescence are formed. As shown in Fig. 17, the tested compound caused an increase in the percentage of cells with decreased  $\Delta\Psi_m$  in the MDA-MB-231 breast cancer cell lines. In the untreated cells (control group), the percentage of cells with depolarized mitochondria was 5.7%. The **3.10** at a lower concentration (5  $\mu$ M) led to a decrease of  $\Delta\Psi_m$  in 15.7% of cell population of tested breast cancer line. Meanwhile, the **3.10** at concentration of 10  $\mu$ M increased this percentage over 2-fold. It was 37.3% of cell population with decreased of  $\Delta\Psi_m$  compared to the control group (untreated cells).

The initiation of the intrinsic apoptosis pathway results in the activation of the caspase 9 [60]. Therefore, we have evaluated the effect of the tested compound **3.10** on the activation of this protein in MDA-MB-231 breast cancer cell lines. The 24 h treatment of cells with the **3.10** induced the elevation in active caspase 9, compared to control. There was 15.0% (5  $\mu$ M) and 32.6% (10  $\mu$ M) cells with active caspase 9 (Fig. 18).

To confirm the results of evaluating the active forms of caspases 8 and 9, we assessed the activity of caspase 3/7. After activation of the initiator caspases (caspases 8 and 9), both apoptotic pathways (intrinsic and extrinsic) converge into a common one and the executive phase of apoptosis begins. During this stage, active executioner caspases, mainly caspase 3, and also caspase 7, are formed [61]. Thus, we evaluated

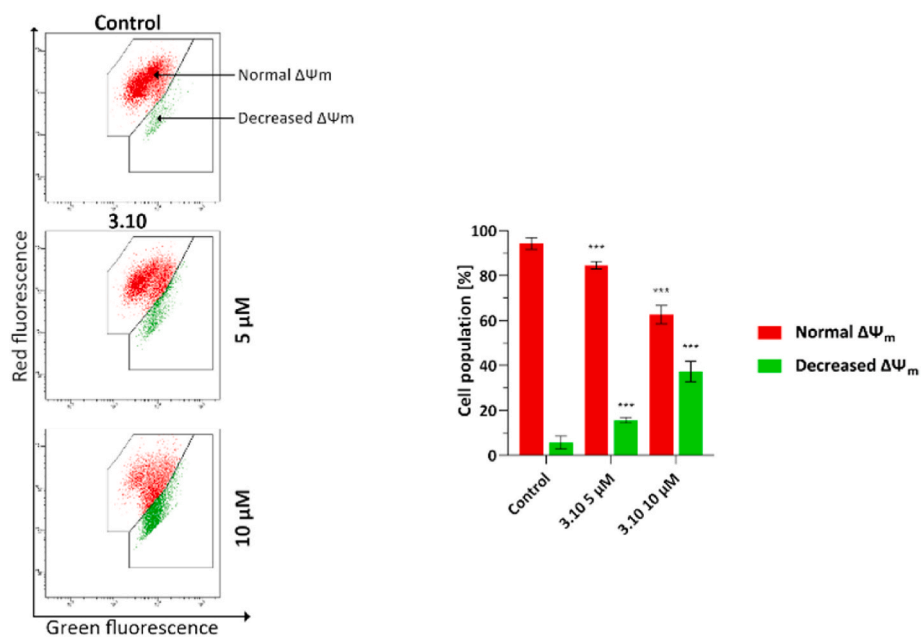


**Fig. 17.** Results of flow cytometry measurement of changes in the mitochondrial membrane potential ( $\Delta\Psi_m$ ) in MDA-MB-231 breast cancer cells after 24 h treatment with **3.10** (concentration 5  $\mu$ M and 10  $\mu$ M). The obtained results are presented as mean values  $\pm$  SD obtained from three independent experiments ( $n = 3$ ) done in duplicate. \*\*\* $p < 0.001$  vs. control group.



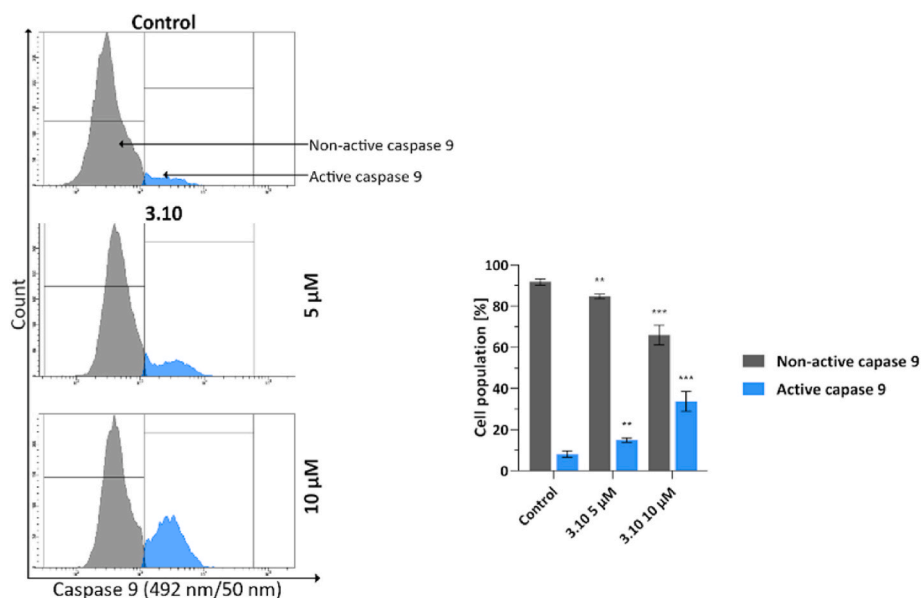


**Fig. 18.** The results of flow cytometry measurement of caspase 9 activity in the MDA-MB-231 breast cancer cells after 24 h incubation with the 3.10 (concentration 5  $\mu$ M and 10  $\mu$ M). The obtained results are presented as mean values  $\pm$  SD obtained from three independent experiments ( $n = 3$ ) done in duplicate. \*\* $p < 0.01$  vs. control group, \*\*\* $p < 0.001$  vs. control group.

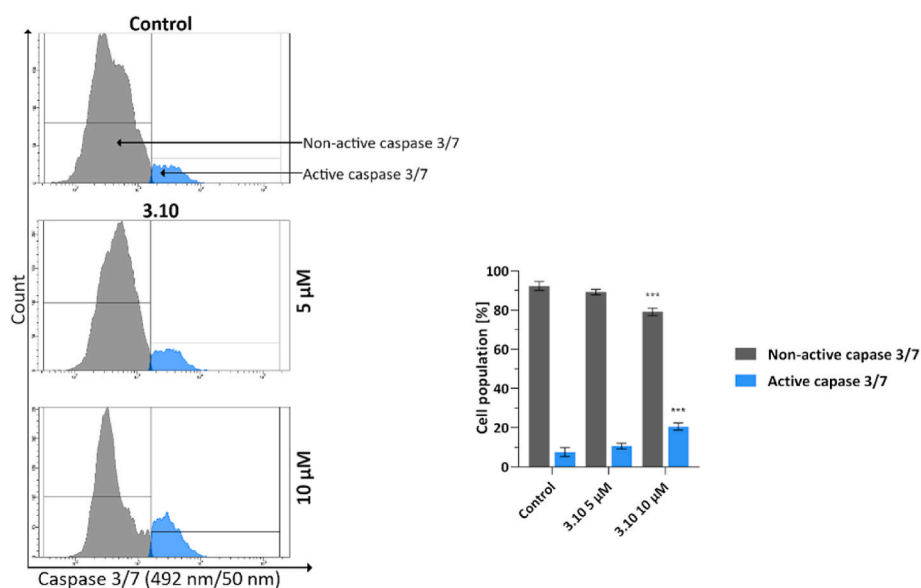


**Fig. 19.** The results of measuring flow cytometry ratio of caspase 3/7 activity in the MDA-MB-231 breast cancer cells treated for 24 h with the 3.10 (concentration 5  $\mu$ M and 10  $\mu$ M). The obtained results are presented as mean values  $\pm$  SD obtained from three independent experiments ( $n = 3$ ) done in duplicate. \*\* $p < 0.01$  vs. control group, \*\*\* $p < 0.001$  vs. control group.

caspase 3/7 activity in the MDA-MB-231 breast cancer cells using flow cytometry after 24 h treatment of cells with the tested compound 3.10. Changes in caspase 3/7 activity were also detected at the action of compound 3.10, in compare with control (Fig. 19). Following treatment with the tested compound resulted in an increase in active form of caspase 3/7 to 10.6% (5  $\mu$ M) and 20.6% (10  $\mu$ M).

The presented results correspond well with other data obtained at the analysis of the apoptotic process and measuring the caspases involved in it. It was demonstrated, that the 3.10 compound induced apoptosis in the MDA-MB-231 breast cancer cells proceeding through two pathways, extrinsic and intrinsic.

## 2.9. Acute toxicity in vivo

Mice treated with Dox demonstrated a rapid time- and dose-dependent loss of body mass. While only slight decrease in body mass of animals was observed after the 1st injection of this drug at a dose of 6.6 mg/kg, the mice lost 10% of their initial mass after the 3<sup>rd</sup> Dox administration (6<sup>th</sup> day of the experiment) when its cumulative dose was 20 mg/kg (Fig. 19). This led to the death of Dox-treated mice on the 8<sup>th</sup> and 13<sup>th</sup> day after the 1st administration of this anthracycline antibiotic. Thus, only 50% (2 out of 4) of animals subjected to doxorubicin treatment survived until the 22<sup>nd</sup> day of experiment, when all animals were euthanized (Fig. 20). It is known that Dox treatment leads to a loss of body mass which is accompanied by fat and skeletal muscle loss, fatigue,

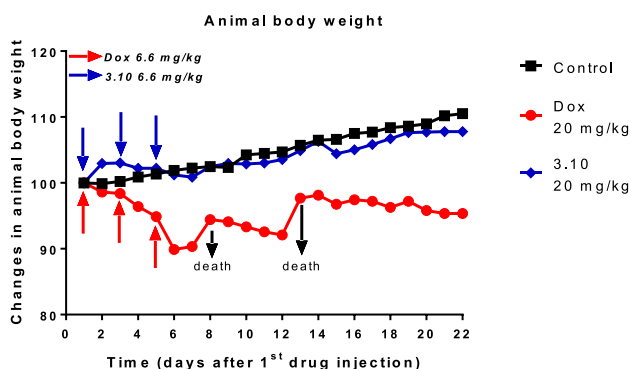


**Fig. 20.** Changes in body mass in control (untreated) C57BL/6 animals and mice treated with the doxorubicin (Dox, 20 mg/kg) or **3.10** compound (20 mg/kg) treatment. Note: Control –  $n=4$ ; Dox –  $n=4$ ; **3.10** –  $n=6$ . ↓ - **3.10** (6.6 mg/ml) injection; ↑ - Dox (6.6 mg/ml) injection.

and anorexia [62,63]. The administration of the **3.10** to C57BL/6 mice in a dose of 20 mg/kg (lethal dose of Dox) was not accompanied by loss of body mass. Animals in this group demonstrated 100% survival rate (Figs. 20 and 21). In contrast to Dox, the action of the compound **3.10** was not characterized by the acute toxic effects.

We detected anemia in Dox-treated mice that was accompanied by 1.4-fold ( $P \leq 0.001$ ) decrease in number of red blood cell and 1.3-fold ( $P \leq 0.01$ ) decrease in hemoglobin level comparing with these parameters in control (untreated) animals (Fig. 21). In addition, Dox (20 mg/kg) caused leukopenia, and on 22nd day of the experiment, the white blood cell count in mice of this group was 1.88 times lower ( $P \leq 0.05$ ) than in animals of control group (Fig. 22). The reason for this might be bone marrow suppression caused by the Dox [64]. The myelosuppression is induced by many chemotherapeutic agents, and doxorubicin is one of the most prominent representatives among them [65–67]. At the same time, the number of red blood cells and white blood cells, as well as the level of hemoglobin in blood of the experimental mice injected with the compound **3.10** did not differ from these indicators in control animals observed on 22nd day after 1st administration of tested compound (Fig. 21).

Relative neutrophil count was 2.3-fold higher ( $P \leq 0.001$ ) and relative lymphocyte count was 1.56-fold lower ( $P \leq 0.001$ ) in the Dox-administered mice than in control animals on 22nd day post 1st injection of this drug. So, the neutrophils to lymphocytes ratio (NLR) in control mice was equal to 0.257, while in Dox-treated animals it was 3.48 times higher, namely 0.894 (Fig. 21, Table 9). These data also demonstrate toxic impacts of Dox on the hematopoietic system (myelosuppression)

and its acute immunotoxicity observed as a significant decrease in number of lymphocytes that could be explained by inhibition of their proliferation or killing by the doxorubicin [68–70].

The compound **3.10** under study slightly reduced the number of lymphocytes (by 1.17 times) and increased the number of neutrophils (by 1.6 times) in blood of treated mice compared to these indicators in control animals on 22nd day of the experiment. It should be noted that the relative number of neutrophils was decreased by 1.4 times ( $P \leq 0.001$ ) and the relative number of lymphocytes was increased by 1.3 times ( $P \leq 0.001$ ) in mice injected with the **3.10** compound, versus to their level in blood of animals treated with the Dox (Fig. 21, Table 9). The neutrophil to lymphocyte ratio in mice injected with the **3.10** compound was 1.8 times higher versus control animals, but it was 1.9 lower than in Dox-treated mice (Table 9). Thus, the compound **3.10** also causes a change in the neutrophil-to-lymphocyte ratio, but to a much lesser extent than the Dox. At the same time, this compound (**3.10**) does not induce a loss of body mass in animals, their rapid death, leukopenia, erythropenia, and a decrease in the level of hemoglobin in blood of treated mice.

At the next stage of study, the organ to body mass indices was analyzed on 22nd day of the experiment in mice injected with saline solution (control vehicle group), doxorubicin (Dox, 20 mg/kg) and **3.10** compound (20 mg/kg). Importantly, there were no statistically significant changes in the mentioned above index for lung, heart, spleen, kidney between control animals and mice treated with the **3.10** compound. Only liver to body mass index in animals injected with the **3.10** was slightly decreased (1.14 times,  $P \leq 0.05$ ) compared to this parameter in control mice (Table 10). In contrast to the effect of the **3.10** (20 mg/kg), Dox significantly affected the weight of the lungs and liver in animals treated with this drug. Thus, the lung- and liver-to-body mass indices in Dox-treated mice were 2.96- and 1.93-fold lower ( $P \leq 0.05$  and  $P \leq 0.001$ ) than in animals from the control group (Table 10). In more detail, the lung-to-body mass index in control mice was equal to  $0.80 \pm 0.09$ , in **3.10**-treated mice –  $0.82 \pm 0.08$  ( $P \leq 0.05$  vs Dox) and in animals of the Dox group –  $0.27 \pm 0.06$  ( $P \leq 0.05$  vs **3.10**). Liver-to-body mass index in control mice was  $5.22 \pm 0.42$ , in **3.10**-injected mice –  $4.54 \pm 0.55$  ( $P \leq 0.05$  vs control,  $P \leq 0.001$  vs Dox) and in Dox-treated animals –  $2.70 \pm 0.04$  ( $P \leq 0.001$  vs control) (Table 9). Lungs and liver mass loss under Dox (20 mg/kg) action may indicate on severe injury of these organs [71].

In order to investigate in more detailed abnormalities in lung and liver tissues, it would be possible to carry out a histopathological analysis of these tissues. However, the non-selectivity of the action of doxorubicin, which leads to damage of several vital organs such as the heart, liver, kidney and others, is a well-known fact [72–75]. In addition, Favreau-Lessard and the group recently found that Dox-treated mice had significantly smaller liver and its histopathological analysis showed atrophy of the hepatic plate with diminished cytoplasmic

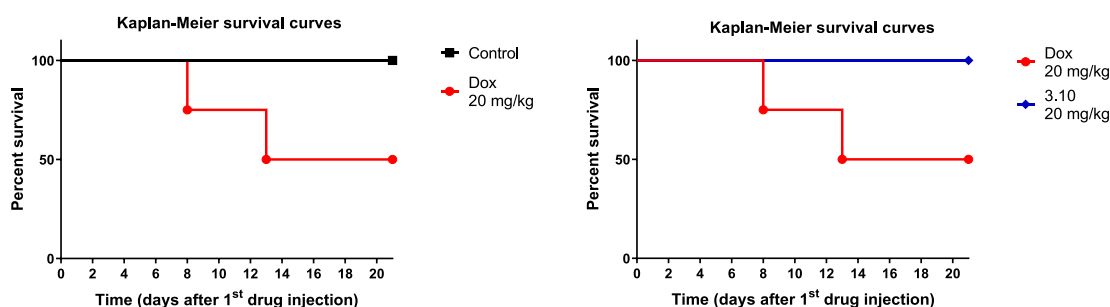


**Fig. 21.** Survival time (Kaplan Meier survival curves) of control (untreated) C57BL/6 mice or animals treated with doxorubicin (Dox, 20 mg/kg) or **3.10** compound (20 mg/kg). Note: Control –  $n=4$ ; Dox –  $n=4$ ; **3.10** –  $n=6$ .

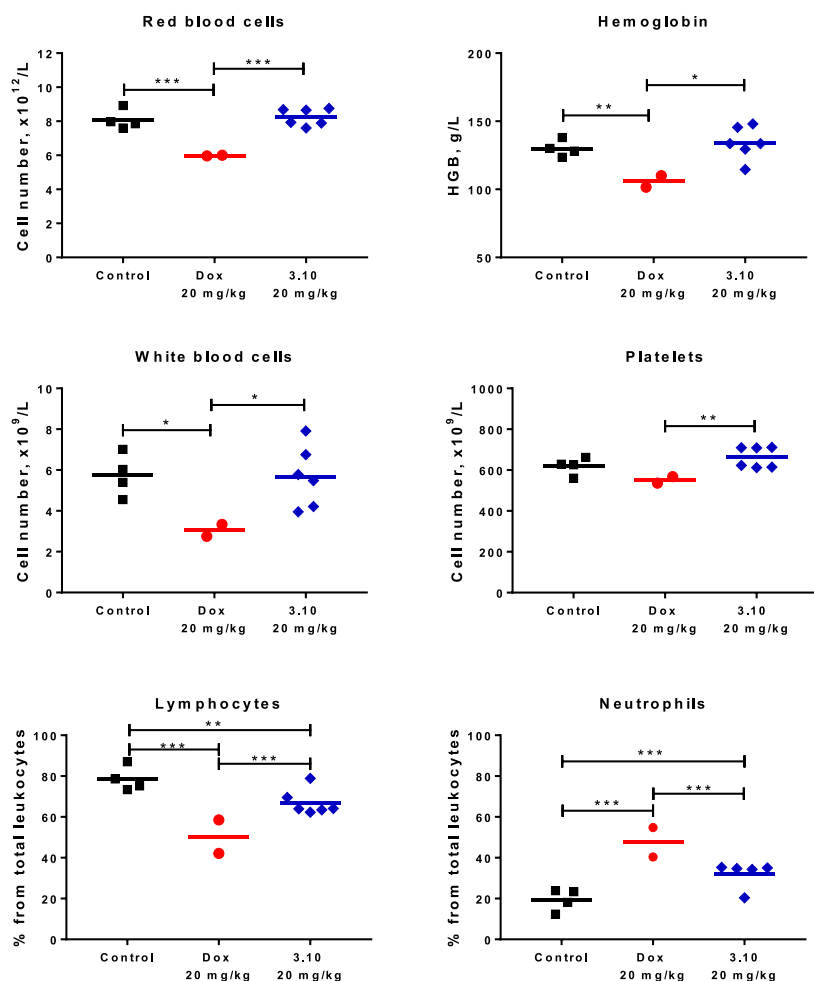


**Fig. 22.** The number of red blood cells (RBC, erythrocytes), platelets (PLT, thrombocytes), white blood cells (WBC, leukocytes), hemoglobin (HGB) level, neutrophil to lymphocyte ratio (NLR) in blood of control (untreated) C57BL/6 mice and animals treated with doxorubicin (Dox, 20 mg/kg) or **3.10** compound (20 mg/kg) on the 22nd day after their first injection or on the 17th day after the last injection of these compounds. Note: Control –  $n=4$ ; Dox –  $n=2$  (because 2 mice had died by that time); **3.10** –  $n=6$ . \* $P \leq 0.05$ , \*\* $P \leq 0.01$ , \*\*\* $P \leq 0.001$  – statistically significant compared to each other.

**Table 9**

Relative neutrophil count (RNC), relative lymphocyte count (RLC) and neutrophil to lymphocyte ratio (NLR) in mice injected with saline solution (control vehicle group), doxorubicin (Dox, 20 mg/kg) and **3.10** compound (20 mg/kg) on 22nd day of the experiment. NLR = RNC/RLC.

	Control Mean $\pm$ SD (n = 4 or 8)	Dox, 20 mg/kg Mean $\pm$ SD (n = 2 or 4)	<b>3.10</b> , 20 mg/kg Mean $\pm$ SD (n = 6 or 12)
Neutrophils, %	19.43 $\pm$ 5.01	45.05 $\pm$ 5.45***	31.21 $\pm$ 6.03***
Lymphocytes, %	78.56 $\pm$ 5.69	50.35 $\pm$ 9.63***	67.05 $\pm$ 6.21***
NLR	0.257	0.894	0.465

**Note:** The level of neutrophils and lymphocytes is expressed as a % total leukocytes (white blood cells, WBC). NLR - neutrophils to lymphocytes ratio; \*\* $P \leq 0.01$ , \*\*\* $P \leq 0.001$  – statistically significant vs control (vehicle) group; \*\*\* $P \leq 0.001$  – statistically significant vs Dox (20 mg/mg) group.

volume and both intracellular and canalicular cholestasis indicating doxorubicin-induced metabolic and toxic liver damage [76]. The toxic effect of Dox on the hematopoietic system confirms the ~2.4-fold decrease in spleen-to-body mass under its action compared to this parameter in control and **3.10** compound-treated mice. More important is that studied compound **3.10** (20 mg/kg) did not change the organ-to-body index for the lung, heart, spleen and kidney compared to these parameters in control mice. Liver-to-body mass index was slightly

**Table 10**

Organ to body mass indices in mice injected with saline solution (control vehicle group), doxorubicin (Dox, 20 mg/kg) and **3.10** compound (20 mg/kg) on 22<sup>nd</sup> day of the experiment. Organ-to-body mass index = (organ mass  $\times$  100)/body weight.

Organs/Groups	Control Mean $\pm$ SD (n = 4)	Dox 20 mg/kg Mean $\pm$ SD (n = 2)	<b>3.10</b> 20 mg/kg Mean $\pm$ SD (n = 6)
Lung	0.80 $\pm$ 0.09	0.27 $\pm$ 0.06*	0.82 $\pm$ 0.08*
Heart	0.62 $\pm$ 0.08	0.34 $\pm$ 0.03	0.51 $\pm$ 0.03
Spleen	0.53 $\pm$ 0.18	0.22 $\pm$ 0.06	0.51 $\pm$ 0.15
Kidney	1.39 $\pm$ 0.09	0.99 $\pm$ 0.05	1.28 $\pm$ 0.12
Liver	5.22 $\pm$ 0.42	2.70 $\pm$ 0.04***	4.54 $\pm$ 0.55* ...

**Note:** \* $P \leq 0.05$ , \*\*\* $P \leq 0.001$  – statistically significant vs control (vehicle) group; ...  $P \leq 0.001$  – statistically significant vs Dox (20 mg/mg) group.

reduced under **3.10** action (Table 10).

### 3. Conclusions

Here, we designed and synthesized new 11-substituted 9-hydroxy-3,5,10,11-tetrahydro-2H-benzo[6,7]thiochromeno[2,3-d][1,3]thiazole-2,5,10-triones **3.1–3.13** using *hetero*-Diels-Alder reaction of 5-ene-4-thio-2-thiazolidinones and 5-hydroxy-1,4-naphthoquinone (juglone) and screened their anticancer potential. The synthesized thiopyrano [2,3-d]thiazoles showed different cytotoxic activity that was dependent

on their structure. The most active compound **3.10** induced extrinsic and intrinsic pathway of apoptosis, increased the percentage of cells in G2/M phase of cell cycle, and reduced the synthesis of DNA and RNA in tumor cells. This compound is capable of interacting with DNA in two different ways: through electrostatic interaction and intercalation. The studied compound **3.10** in dose 20 mg/kg did not cause toxic effects in the organism of C57BL/6 mice. Thus, although traditional antitumor drug doxorubicin and the created compound **3.10** possess comparable anticancer activity, the novel drug-like medicine demonstrates prominent bio-tolerance, while the doxorubicin demonstrates severe adverse effects *in vivo*.

## 4. Materials and methods

### 4.1. General information

Commercially available reagents and anhydrous solvents were used without further purification. Melting points were measured on a Cole-Parmer Electrothermal IA9200 melting point apparatus. The elemental analyses were performed using the Thermo Scientific FlashSmart Elemental Analyzer. The  $^1\text{H}$  and  $^{13}\text{C}$  NMR spectra were recorded on Varian Gemini ( $^1\text{H}$  at 400 and  $^{13}\text{C}$  at 100 MHz) instrument in DMSO- $d_6$ . Chemical shifts ( $\delta$ ) are given in ppm units relative to tetramethylsilane as reference (0.00). TLC checked the purity of all obtained compounds on Silufol-254 plates (Eluent EtOAc/Benzene 1:2). 4-Thioxo-2-thiazolidinone was prepared according literature procedure from 2,4-thiazolidinone [77]. The 5-ene-4-thioxo-2-thiazolidinones were synthesized previously [78].

Synthesis of 9-hydroxy-11-substituted-3,11-dihydro-2H-benzo[6,7]thiochromeno[2,3-d]thiazole-2,5,10-triones.

A mixture of appropriate 5-ene-4-thioxo-2-thiazolidinone (10 mmol) and 5-hydroxy-1,4-naphthoquinone (20 mmol) was refluxed for 1 h with a catalytic amount of hydroquinone (2–3 mg) in glacial acetic acid (10 mL), and then left overnight at room temperature. The precipitated crystals were filtered off, washed with methanol (5–10 mL), and recrystallized from appropriate solvent.

#### 4.1.1. 11-(5-Chloro-2-hydroxyphenyl)-9-hydroxy-3,11-dihydro-2H-benzo[6,7]thiochromeno[2,3-d]thiazole-2,5,10-trione (3.1)

Yield 70%, mp > 350 °C (AcOH).  $^1\text{H}$  NMR (400 MHz, DMSO- $d_6$ ):  $\delta$  5.69 (s, 1H, CH), 6.82 (t, 1H,  $J = 7.2$  Hz, arom.), 7.07 (d, 1H,  $J = 8.9$  Hz, arom.), 7.16–7.24 (m, 1H, arom.), 7.32 (s, 1H, arom.), 7.61 (d, 1H,  $J = 8.1$  Hz, arom.), 7.72 (d, 1H,  $J = 9.0$  Hz, arom.), 10.31 (s, 1H, OH), 11.64 (s, 1H, OH), 11.78 (s, 1H, NH).  $^{13}\text{C}$  NMR (100 MHz, DMSO- $d_6$ ):  $\delta$  33.5, 94.1, 116.8, 121.2, 123.0, 125.0, 127.4, 128.2, 130.9, 133.5, 136.4, 139.5, 141.4, 143.7, 153.4, 158.2, 160.4, 175.0, 184.5. ESI-MS  $m/z$  442/444 (M+H) $^+$ . Anal. Calcd for  $\text{C}_{20}\text{H}_{10}\text{ClNO}_5\text{S}_2$ : C, 54.12; H, 2.27; N, 3.16. Found: C, 54.28; H, 2.11; N, 3.05.

#### 4.1.2. 11-(4-Bromophenyl)-9-hydroxy-3,11-dihydro-2H-benzo[6,7]thiochromeno[2,3-d]thiazole-2,5,10-trione (3.2)

Yield 62%, mp 240–242 °C (AcOH).  $^1\text{H}$  NMR (400 MHz, DMSO- $d_6$ ):  $\delta$  5.52 (s, 1H, CH), 7.28–7.37 (m, 2H, arom.), 7.48 (t, 2H,  $J = 6.8$  Hz, arom.), 7.58 (d, 1H,  $J = 7.2$  Hz, arom.), 7.70 (d, 1H,  $J = 8.0$  Hz, arom.), 11.67 (s, 1H, OH), 11.94 (s, 1H, NH).  $^{13}\text{C}$  NMR (100 MHz, DMSO- $d_6$ ):  $\delta$  29.7, 99.1, 107.8, 115.7, 119.3, 120.8, 125.2, 129.9, 131.7, 134.7, 136.5, 141.4, 146.2, 156.1, 160.5, 170.5, 179.8. ESI-MS  $m/z$  471/473 (M+H) $^+$ . Anal. Calcd for  $\text{C}_{20}\text{H}_{10}\text{BrNO}_4\text{S}_2$ : C, 50.86; H, 2.13; N, 2.97. Found: C, 51.01; H, 2.23; N, 3.06.

#### 4.1.3. 11-(4-Chlorophenyl)-9-hydroxy-3,11-dihydro-2H-benzo[6,7]thiochromeno[2,3-d]thiazole-2,5,10-trione (3.3)

Yield 68%, mp > 350 °C (AcOH).  $^1\text{H}$  NMR (400 MHz, DMSO- $d_6$ ):  $\delta$  5.54 (s, 1H, CH), 7.30–7.42 (m, 4H, arom.), 7.59 (d, 1H,  $J = 7.4$  Hz, arom.), 7.71 (m, 1H, arom.), 11.68 (s, 1H, OH), 11.94 (s, 1H, NH).  $^{13}\text{C}$  NMR (100 MHz, DMSO- $d_6$ ):  $\delta$  28.6, 84.7, 101.0, 116.2, 119.3, 125.2,

126.0, 128.8, 129.5, 133.1, 136.5, 141.5, 150.2, 163.6, 169.6, 175.2, 179.5. ESI-MS  $m/z$  426/428 (M+H) $^+$ . Anal. Calcd for  $\text{C}_{20}\text{H}_{10}\text{ClNO}_4\text{S}_2$ : C, 56.14; H, 2.36; N, 3.27. Found: C, 56.28; H, 2.20; N, 3.17.

#### 4.1.4. 9-Hydroxy-11-(4-methoxyphenyl)-3,11-dihydro-2H-benzo[6,7]thiochromeno[2,3-d]thiazole-2,5,10-trione (3.4)

Yield 71%, mp 234–236 °C (AcOH).  $^1\text{H}$  NMR (400 MHz, DMSO- $d_6$ ): 3.69 (s, 3H, OCH $_3$ ), 5.43 (s, 1H, CH), 6.85 (d, 2H,  $J = 8.4$  Hz, arom.), 7.27 (d, 2H,  $J = 8.4$  Hz, arom.), 7.34 (d, 1H,  $J = 8.5$  Hz, arom.), 7.58 (d, 1H,  $J = 7.4$  Hz, arom.), 7.71 (t, 1H,  $J = 8.0$  Hz, arom.), 11.74 (s, 1H, OH), 11.90 (s, 1H, NH).  $^{13}\text{C}$  NMR (100 MHz, DMSO- $d_6$ ):  $\delta$  35.3, 47.4, 92.7, 101.3, 109.1, 114.6, 125.9, 129.9, 133.1, 135.9, 139.4, 142.1, 144.4, 148.1, 153.9, 159.2, 170.3, 174.2, 177.6. ESI-MS  $m/z$  424 (M+H) $^+$ . Anal. Calcd for  $\text{C}_{21}\text{H}_{13}\text{NO}_5\text{S}_2$ : C, 59.56; H, 3.09; N, 3.31. Found: C, 59.41; H, 2.92; N, 3.49.

#### 4.1.5. 11-(4-(Dimethylaminophenyl)-9-hydroxy-3,11-dihydro-2H-benzo[6,7]thiochromeno[2,3-d]thiazole-2,5,10-trione (3.5)

Yield 67%, mp > 350 °C (DMF:EtOH).  $^1\text{H}$  NMR (400 MHz, DMSO- $d_6$ ): 2.80 (s, 6H, N(CH $_3$ ) $_2$ ), 5.29 (s, 1H, CH), 6.59 (d, 2H,  $J = 8.2$  Hz, arom.), 7.08 (d, 2H,  $J = 8.0$  Hz, arom.), 7.49–7.57 (m, 2H, arom.), 7.78 (t, 1H,  $J = 7.9$  Hz, arom.), 11.54 (s, 1H, OH), 11.80 (s, 1H, NH).  $^{13}\text{C}$  NMR (100 MHz, DMSO- $d_6$ ):  $\delta$  30.7, 48.0, 100.8, 112.5, 117.4, 120.0, 123.3, 128.1, 132.0, 135.7, 137.5, 138.1, 141.6, 146.2, 149.4, 159.7, 162.7, 167.2, 176.9. ESI-MS  $m/z$  437 (M+H) $^+$ . Anal. Calcd for  $\text{C}_{22}\text{H}_{16}\text{N}_2\text{O}_4\text{S}_2$ : C, 60.54; H, 3.69; N, 6.42. Found: C, 60.43; H, 3.77; N, 6.58.

#### 4.1.6. 9-Hydroxy-11-styryl-3,11-dihydro-2H-benzo[6,7]thiochromeno[2,3-d]thiazole-2,5,10-trione (3.6)

Yield 64%, mp > 350 °C (DMF:EtOH).  $^1\text{H}$  NMR (400 MHz, DMSO- $d_6$ ):  $\delta$  6.37 (s, 1H, CH), 7.06–7.39 (m, 5H, CH, arom.), 7.40–7.52 (m, 3H, CH, arom.), 7.76 (d, 1H,  $J = 7.4$  Hz, arom.), 7.93 (t, 1H,  $J = 7.8$  Hz, arom.), 11.02 (s, 1H, OH), 11.12 (s, 1H, NH).  $^{13}\text{C}$  NMR (100 MHz, DMSO- $d_6$ ):  $\delta$  36.0, 98.6, 117.1, 118.8, 122.2, 122.5, 125.8, 128.3, 130.1, 132.3, 136.3, 137.8, 139.4, 141.3, 161.3, 163.4, 169.3, 171.4, 174.5. ESI-MS  $m/z$  420 (M+H) $^+$ . Anal. Calcd for  $\text{C}_{22}\text{H}_{13}\text{NO}_4\text{S}_2$ : C, 62.99; H, 3.12; N, 3.34. Found: C, 63.09; H, 3.02; N, 3.50.

#### 4.1.7. 9-Hydroxy-11-(2-nitrostyryl)-3,11-dihydro-2H-benzo[6,7]thiochromeno[2,3-d]thiazole-2,5,10-trione (3.7)

Yield 77%, mp > 350 °C (DMF:EtOH).  $^1\text{H}$  NMR (400 MHz, DMSO- $d_6$ ):  $\delta$  5.21 (s, 1H, CH), 6.31 (m, 1H, CH), 6.81 (d, 1H,  $J = 13.8$  Hz, CH), 7.36–7.39 (m, 1H, arom.), 7.45–7.49 (m, 1H, arom.), 7.58–7.61 (m, 2H, arom.), 7.67–7.70 (m, 1H, arom.), 7.88–7.92 (m, 2H, arom.), 11.87 (s, 1H, OH), 11.97 (s, 1H, NH).  $^{13}\text{C}$  NMR (100 MHz, DMSO- $d_6$ ):  $\delta$  35.8, 87.1, 110.0, 115.1, 123.0, 124.3, 126.2, 126.7, 128.5, 133.1, 136.7, 137.6, 139.7, 141.3, 148.5, 148.7, 162.7, 176.5, 177.0, 177.7. ESI-MS  $m/z$  465 (M+H) $^+$ . Anal. Calcd for  $\text{C}_{22}\text{H}_{12}\text{N}_2\text{O}_6\text{S}_2$ : C, 56.89; H, 2.60; N, 6.03. Found: C, 56.70; H, 2.41; N, 6.14.

#### 4.1.8. 9-Hydroxy-11-(2-phenylprop-1-en-1-yl)-3,11-dihydro-2H-benzo[6,7]thiochromeno[2,3-d]thiazole-2,5,10-trione (3.8)

Yield 79%, mp > 350 °C (DMF:EtOH).  $^1\text{H}$  NMR (400 MHz, DMSO- $d_6$ ):  $\delta$  0.96 (s, 3H, CH $_3$ ), 5.48 (s, 1H, CH), 7.26–7.33 (m, 4H, CH, arom.), 7.52 (m, 3H, arom.), 7.76 (d, 1H,  $J = 7.8$  Hz, arom.), 7.99 (t, 1H,  $J = 8.0$  Hz, arom.), 11.06 (s, 1H, OH), 11.22 (s, 1H, NH).  $^{13}\text{C}$  NMR (100 MHz, DMSO- $d_6$ ):  $\delta$  17.1, 31.4, 84.6, 106.9, 116.4, 118.6, 120.3, 124.4, 126.4, 130.9, 134.1, 134.3, 136.3, 136.8, 143.7, 150.4, 150.7, 162.8, 176.2, 178.8, 182.1. ESI-MS  $m/z$  434 (M+H) $^+$ . Anal. Calcd for  $\text{C}_{23}\text{H}_{15}\text{NO}_4\text{S}_2$ : C, 63.73; H, 3.49; N, 3.23. Found: C, 63.55; H, 3.67; N, 3.37.

#### 4.1.9. 9-Hydroxy-11-(thiophen-2-yl)-3,11-dihydro-2H-benzo[6,7]thiochromeno[2,3-d]thiazole-2,5,10-trione (3.9)

Yield 71%, mp 244–246 °C (AcOH).  $^1\text{H}$  NMR (400 MHz, DMSO- $d_6$ ):  $\delta$



5.89 (s, 1H, CH), 6.92 (d, 1H,  $J = 7.2$  Hz, arom.), 6.96–7.02 (m, 1H, thiophen.), 7.33–7.41 (m, 2H, arom., thiophen.), 7.54–7.62 (m, 1H, thiophen.), 7.72 (d, 1H,  $J = 8.2$  Hz, arom.), 11.76 (s, 1H, OH), 12.01 (s, 1H, NH).  $^{13}\text{C}$  NMR (100 MHz, DMSO- $d_6$ ):  $\delta$  33.6, 102.2, 114.2, 117.4, 119.4, 125.4, 125.8, 127.3, 129.7, 134.7, 136.7, 140.5, 143.9, 147.0, 160.6, 162.0, 169.7, 176.6. ESI-MS  $m/z$  400 (M+H) $^+$ . Anal. Calcd for  $\text{C}_{18}\text{H}_9\text{NO}_4\text{S}_3$ : C, 54.12; H, 2.27; N, 3.51. Found: C, 54.23; H, 2.11; N, 3.67.

#### 4.1.10. 11-(Furan-2-yl)-9-hydroxy-3,11-dihydro-2H-benzo[6,7]thiochromeno[2,3-d]thiazole-2,5,10-trione (3.10)

Yield 69%, mp > 350 °C (AcOH).  $^1\text{H}$  NMR (400 MHz, DMSO- $d_6$ ):  $\delta$  5.67 (s, 1H, CH), 6.30–6.36 (m, 2H, arom.), 7.36 (d, 1H,  $J = 8.2$  Hz, arom.), 7.53–7.56 (m, 1H, arom.) 7.59 (d, 1H,  $J = 7.3$  Hz, arom.), 7.73 (t, 1H,  $J = 7.9$  Hz, arom.), 11.73 (s, 1H, OH), 11.98 (s, 1H, NH).  $^{13}\text{C}$  NMR (100 MHz, DMSO- $d_6$ ):  $\delta$  33.3, 105.5, 107.6, 111.3, 114.6, 117.3, 119.8, 125.7, 131.5, 132.9, 137.0, 143.3, 144.5, 152.7, 161.0, 180.9, 180.2, 184.6. ESI-MS  $m/z$  384 (M+H) $^+$ . Anal. Calcd for  $\text{C}_{18}\text{H}_9\text{NO}_5\text{S}_2$ : C, 56.39; H, 2.37; N, 3.65. Found: C, 56.50; H, 2.49; N, 3.51.

#### 4.1.11. 11-(Furan-2-yl)-3,11-dihydro-2H-benzo[6,7]thiochromeno[2,3-d]thiazole-2,5,10-trione (3.11)

Yield 73%, mp 238–240 °C (DMF: EtOH).  $^1\text{H}$  NMR (400 MHz, DMSO- $d_6$ ):  $\delta$  5.90 (s, 1H, CH), 6.90 (d, 1H,  $J = 4.4$  Hz, furan.), 6.93–6.98 (m, 1H, furan.), 7.35–7.40 (m, 1H, furan.), 7.83–7.91 (m, 2H, arom.), 7.97–8.04 (m, 2H, arom.), 12.00 (s, 1H, NH).  $^{13}\text{C}$  NMR (100 MHz, DMSO- $d_6$ ):  $\delta$  34.1, 106.4, 112.5, 119.3, 125.7, 127.2, 136.8, 136.8, 139.7, 141.4, 144.1, 149.8, 157.4, 168.5, 177.4, 181.7. ESI-MS  $m/z$  368 (M+H) $^+$ . Anal. Calcd for  $\text{C}_{18}\text{H}_9\text{NO}_4\text{S}_2$ : C, 58.85; H, 2.47; N, 3.81. Found: C, 58.74; H, 2.40; N, 3.92.

#### 4.1.12. 9-Hydroxy-11,11-dimethyl-3,11-dihydro-2H-benzo[6,7]thiochromeno[2,3-d]thiazole-2,5,10-trione (3.12)

Yield 79%, mp > 350 °C (DMF:MeOH).  $^1\text{H}$  NMR (400 MHz, DMSO- $d_6$ ):  $\delta$  2.72 (s, 3H, CH $_3$ ), 2.88 (s, 3H, CH $_3$ ), 7.51 (d, 1H,  $J = 8.4$  Hz, arom.), 7.75 (m, 1H, arom.), 7.93 (m, 1H, arom.), 11.60 (s, 1H, OH), 12.58 (s, 1H, NH).  $^{13}\text{C}$  NMR (100 MHz, DMSO- $d_6$ ):  $\delta$  20.8, 24.2, 96.4, 114.4, 118.8, 123.8, 127.3, 134.1, 137.0, 151.5, 157.4, 163.9, 173.3, 175.1, 179.1. ESI-MS  $m/z$  346 (M+H) $^+$ . Anal. Calcd for  $\text{C}_{22}\text{H}_{15}\text{NO}_4\text{S}_2$ : C, 62.69; H, 3.59; N, 3.32. Found: C, 62.79; H, 3.45; N, 3.21.

#### 4.1.13. Synthesis of 9-hydroxy-11-phenethyl-3,11-dihydro-2H-benzo[6,7]thiochromeno[2,3-d]thiazole-2,5,10-trione (3.13)

A mixture of isorhodanine (5 mmol), phenylpropionaldehyde (5.5 mmol), and 1,4-naphthoquinone (10 mmol) was heated at reflux for 2 h in MeCN (10 mL) in the presence of the catalytic amount of ethylenediammonium diacetate (EDDA). After cooling, the precipitate was filtered off, washed, and recrystallized from a mixture DMF: EtOH (1:2). Yield 65%, mp > 350 °C.  $^1\text{H}$  NMR (400 MHz, DMSO- $d_6$ ):  $\delta$  2.37 (m, 2H, CH $_2$ ), 2.62 (m, 2H, CH $_2$ ), 5.22 (s, 1H, CH), 7.38 (m, 2H, arom.), 7.48 (m, 2H, arom.), 7.60 (m, 1H, arom.), 7.68 (m, 1H, arom.), 7.90 (m, 1H, arom.), 8.08 (m, 1H, arom.), 11.87 (s, 1H, OH). 11.99 (s, 1H, NH).  $^{13}\text{C}$  NMR (100 MHz, DMSO- $d_6$ ):  $\delta$  21.5, 28.2, 32.8, 95.3, 110.7, 122.0, 122.6, 123.9, 125.8, 126.6, 128.2, 129.7, 132.0, 137.5, 139.7, 145.5, 165.6, 171.0, 186.9, 188.8. ESI-MS  $m/z$  422 (M+H) $^+$ . Anal. Calcd for  $\text{C}_{18}\text{H}_{13}\text{NO}_3\text{S}_2$ : C, 60.83; H, 3.69; N, 3.94. Found: C, 61.00; H, 3.76; N, 4.04.

### 4.2. Crystal structure determination of 3.4

Compound 3.4 was recrystallized from DMF by slow evaporation at room temperature.

Crystal data.  $\text{C}_{21}\text{H}_{13}\text{NO}_5\text{S}_2$ ,  $\text{C}_3\text{H}_7\text{NO}$ ,  $M_r = 496.54$ , orthorhombic, space group  $Pbca$ ,  $a = 13.1978(3)$ ,  $b = 13.9935(3)$ ,  $c = 23.9945(5)$  Å,  $V = 4431.39(17)$  Å $^3$ ,  $Z = 8$  ( $Z' = 1$ ),  $D_{\text{calc}} = 1.489$  g/cm $^3$ ,  $\mu = 2.578$  mm $^{-1}$ ,  $T = 130.0(1)$  K.

**Data collection.** A brown crystal of undefined shape (DMF),  $0.32 \times 0.08 \times 0.05$  mm, was used to record 14669 (Cu  $K\alpha$ -radiation,  $\theta_{\text{max}} = 76.65^\circ$ ) intensities on a Rigaku SuperNova Dual Atlas diffractometer using mirror monochromatized Cu  $K\alpha$ -radiation from a high-flux microfocus source ( $\lambda = 1.54184$  Å). Accurate unit cell parameters were determined by least-squares techniques from the  $\theta$  values of 7698 reflections,  $\theta$  range  $4.92$ – $76.44^\circ$ . The data were corrected for Lorentz, polarization and for absorption effects [79]. The 4603 total unique reflections ( $R_{\text{int}} = 0.0254$ ) were used for structure determination.

**Structure solution and refinement.** The structure was solved by dual space algorithm (SHELXT) [80], and refined against  $F^2$  for all data (SHELXL) [81]. The positions of the H atoms bonded to N and O atoms were obtained from the difference Fourier maps and were refined freely. The remaining H atoms were positioned geometrically and were refined within the riding model approximation: C–H = 0.98 Å (CH $_3$ ), 1.00 Å (Csp $^3$ H), 0.95 Å (Csp $^2$ H) and  $U_{\text{iso}}(\text{H}) = 1.2U_{\text{eq}}(\text{C})$  or  $1.5U_{\text{eq}}(\text{C})$  for methyl H atoms. The methyl groups were refined as rotatable rigid groups. Final refinement converged with  $R = 0.0428$  (for 4068 data with  $F^2 > 4\sigma(F^2)$ ),  $wR = 0.1189$  (on  $F^2$  for all data), and  $S = 1.147$  (on  $F^2$  for all data). The largest difference peak and hole was 0.593 and  $-0.243$  eÅ $^{-3}$ . The molecular illustration was drawn using ORTEP-3 for Windows [82]. The material for publication was prepared using and PLATON [39]. Software used to prepare material for publication was WINGX [82], OLEX2 [83] and PLATON [39].

The supplementary crystallographic data are deposited at the Cambridge Crystallographic Data Centre (CCDC), 12 Union ROAD, Cambridge CB2 1EZ (UK) [phone, (+44) 1223/336–408; fax, (+44) 1223/336–033; e-mail, [deposit@ccdc.cam.ac.uk](mailto:deposit@ccdc.cam.ac.uk); World Wide Web, <http://www.ccdc.cam.ac.uk> (deposition no. CCDC 2235052)].

### 4.3. NCI anticancer screening in vitro

Primary anticancer assay was performed on a panel of approximately sixty human tumor cell lines derived from nine neoplastic diseases, in accordance with the protocol of the Drug Evaluation Branch, National Cancer Institute, Bethesda [41–43]. Tested compounds were added to the culture at a single concentration ( $10^{-5}$  M) and incubated for 48 h. The cytotoxic and/or growth inhibitory effects of for each tested compound were evaluated using sulforhodamineB (SRB) assay. Results was reported as the percent of growth of the treated cells compared to the untreated control cells. The most active selected compounds were tested *in vitro* against the full panel of human tumor cell lines at concentrations ranging from  $10^{-4}$  to  $10^{-8}$  M. 48-h drug exposure protocol was followed. SRB assay was used to estimate cell viability or growth.

Using absorbance measurements [time zero ( $T_z$ ), control growth in the absence of drug ( $C$ ), and test growth in the presence of drug ( $T_i$ )], the percentage growth was calculated for each drug concentration. Percentage growth inhibition was calculated as:

$$[(T_i - T_z) / (C - T_z)] \times 100 \text{ for concentrations for which } T_i \geq T_z$$

$$[(T_i - T_z) / T_z] \times 100 \text{ for concentrations for which } T_i < T_z.$$

Dose response parameters ( $GI_{50}$ , TGI) were calculated for each compound. Growth inhibition of 50% ( $GI_{50}$ ) was calculated from  $[(T_i - T_z) / (C - T_z)] \times 100 = 50$ , which is the drug concentration resulting in a 50% lower net protein increase in the treated cells (measured by SRB staining) as compared to the net protein increase seen in the control cells. The drug concentration resulting in total growth inhibition (TGI) was calculated from  $T_i = T_z$ . Values were calculated for each of these parameters if the level of activity was reached; however, if the effect was not reached or was excessive, the value for that parameter was expressed as more or less than the maximum or minimum concentration tested. The lowest values were obtained with the most sensitive cell lines. Compounds having  $GI_{50}$  values  $\leq 100$   $\mu\text{M}$  were declared to be active.

#### 4.4. Compare analysis and docking assays

NCI COMPARE analysis algorithm ([https://dtp.cancer.gov/database\\_s\\_tools/compare.htm](https://dtp.cancer.gov/database_s_tools/compare.htm)) indicates a correlation of the anticancer activity to nearly 60 human tumor cell lines types between the tested compound with previously tested anticancer agents. This statistical approach is used to predict and identify the mechanisms of action of synthetic and natural products. Therefore, the *in vitro* antitumor screening of **3.10** was analyzed using COMPARE algorithm against the NCI different database at the GI<sub>50</sub> levels.

The optimization geometry of **3.10** was pre-performed using the MM + quantum mechanics algorithm, followed by final optimization using PM3 semi-empirical technique by HyperChem 7.5 package. Autodock Tools v.4.2.6 was used for protein-ligand docking with the NMR structures of TGFβ (PDB code 1VJY), topoisomerase I (PDB code 1T8I), topoisomerase II (PDB code 3QX3) and human dihydroorotate dehydrogenase (hDHODH) (PDB code 6LP7) with using the enhanced Lamarckian Genetic Algorithm parameters [84], where GA runs was set to 100 and population size was increased to 300; other parameters were considered as their default values. The tested enzymes were set to be rigid, while the **3.10** was set to be free to rotate. A grid box of 60 × 60 × 60 points with 0.375 Å spacing was defined by centering on the ligand in the active site. The lowest energy conformations were selected as the resultant docked positions. The root mean square deviation (RMSD) calculation [85] was used for evaluating the possibility of the selected docking parameters to reproduce the interaction of the native ligands with the selected enzymes. Poses with RMSD less than 2.0 Å allow considering the performed docking as valid. In addition, doxorubicin was used for cross-docking assays. The Discovery Studio Visualizer has generated molecular representations of each protein-ligand complexes.

#### 4.5. Reduced glutathione (GSH) level assay

In model experiments, 1 mM of GSH and 1 mM of compounds in 0.1 M phosphate buffer (pH 7.4) were incubated for 1 h at 37 °C, and then the level of GSH was determined spectrophotometrically at 412 nm based on the reduction of 5,5'-dithio-bis(2-nitrobenzoic acid) to form the yellow derivative 5'-thio-2-nitrobenzoic acid. Oxidized glutathione GSSG in samples was reduced to GSH with sodium borohydride [86].

#### 4.6. Cell culture

MCF-7 human breast adenocarcinoma cell line, HCT-116 colon adenocarcinoma cell line, KB3-1 human cervix adenocarcinoma cell line, Jurkat human T lymphocyte cell line, K562 human chronic myelogenous leukemia cell line, human keratinocytes of HaCaT line, murine macrophage-like cell line J774.2, and NIH/3T3 mouse embryonic fibroblasts were kindly provided by a Collection at the Institute of Molecular Biology and Genetics, National Academy of Sciences of Ukraine (Kyiv, Ukraine) received those cells from the American Type Culture Collection (ATCC). The p53-deficient HCT-116 p53<sup>-/-</sup> colon cancer cells were a kind gift from a Collection of the Institute for Cancer Research at Vienna Medical University (Vienna, Austria). Cells were cultivated in the DMEM or RPMI-1640 medium supplemented with 10% of fetal bovine serum (all were purchased from Biowest, France) in the CO<sub>2</sub> thermostat at 37 °C in atmosphere of 95% air and 5% CO<sub>2</sub>.

The study protocols with human lymphocytes isolated from peripheral blood of adult healthy donor and patients with acute and chronic leukemia were approved by Ethics Committee of the Institute of Cell Biology of National Academy of Sciences of Ukraine (protocols No 2 from January 27, 2019 and No 2 from October 7, 2020), and with written consent of donor. Lymphocytes of human peripheral blood were isolated from blood consisting of anti-coagulant sodium heparin solution 10 U/mL (B.BRAUN MEDICAL, S.A., Spain) from a donor on density gradient of Gradisol G (Polfa, Poland), as described. Briefly, the blood/Gradisol G mixture (1:1) was centrifuged at 400×g at room temperature

for 30 min. The cells were washed in the phosphate buffered saline (PBS). The residual erythrocytes were lysed in hypotonic solution. Lymphocytes were cultured in the RPMI-1640 medium supplemented with 20% of fetal bovine serum (both were purchased from Biowest, France) at 95% air and 5% CO<sub>2</sub> [87].

#### 4.7. MTT assay for measuring cells viability

The sensitivity of tumor, normal and pseudo-normal cells to new heterocyclic derivatives was evaluated as described [87] using MTT (3-[4,5-dimethylthiazol-2-yl]-2,5-diphenyl tetrazolium bromide) test (Sigma-Aldrich, USA). The 3500–4000 adherent or 15,000 suspension cells per well were seeded in 96-well plates according to ATCC recommendation in 100 μL DMEM or RPMI-1640 complete medium (Sigma-Aldrich, Burlington, MA, USA), and incubated for 72 h at 37 °C in CO<sub>2</sub>-incubator with studied compounds at final concentrations of 1, 10, 50 μM. After incubation, MTT reagent were added to the cells according with manufacture recommendation and incubated for the next 4 h. Crystals of formazan were dissolved in the dimethylsulfoxide (DMSO), and the reaction absorbance was measured by an Absorbance Reader BioTek ELx800 (BioTek Instruments, Inc., Winooski, VT, USA). The half maximal inhibitory concentration value (IC<sub>50</sub>) was calculated by GraphPad Prism 6 software (San Diego, CA, USA) using nonlinear regression.

#### 4.8. Clonogenic assay

Cells were plated in 6-well plates (10<sup>6</sup> cells in 1.5 ml growth medium per well) and left to recover and attach for 24 h in the incubator. Next day it was added compound **3.10** in indicated concentrations, Dox was used as positive control. After 3 days, the cells were fixed with methanol for 20 min at 4 °C and stained with crystal violet 5 (0.01% in PBS). The fluorescence of crystal violet was detected by the Absorbance Reader BioTek ELx800 (BioTek Instruments, Inc., Winooski, VT, USA). Quantification was done by ImageJ software. The received data was visualized as dose-response surviving fraction curves by Graph Pad Prism 6 software (Graph Pad software, USA). All calculations were done as described by Ref. [88].

#### 4.9. Methyl green DNA intercalation test

Compounds **3.1–3.13** juglone and **2.10** were also investigated for the ability to intercalate DNA by the Methyl green assay. Salmon sperm DNA (50 μg/mL) was incubated for 1 h at 37°C with 15 μl Methyl green solution (1 mg/ml in H<sub>2</sub>O). Tested compounds were added at concentration 10 μM/ml and incubated at 37 °C in the dark for 24 h. The total volume of the samples was 1 ml in the end. Absorption of Methyl green was measured at 630 nm with a fluorescence reader Plate Reader BioTek (USA). As a positive control was used doxorubicin [89].

#### 4.10. Study of DNA-binding ability of synthesized compounds

Salmon Sperm DNA (Sigma-Aldrich, USA) was diluted in distilled water at 4 °C for 24 h in stock concentration 1.65 mg/mL. Tested compounds were dissolved in acetone (stock solution concentration 5 mM/mL). DNA (5 μl, 8.27 μg) was incubated with the test compound in dH<sub>2</sub>O for 1 h at 37 °C. Following incubation of DNA and compound, KMnO<sub>4</sub> was added to a final concentration of 0.3 mM. A range of concentrations (3, 6, 12, 24 μM/mL) were tested for each compound and the results expressed as the change in absorbance (ΔAbs) during the reaction with KMnO<sub>4</sub> between zero time zero and selected time points afterward (1, 2, and 3 h) at the specific wavelength 405 nm. Appropriate controls of DNA alone and compounds alone were included and these values subtracted from the test sample to provide the net change in absorbance (NetΔAbs).

Net A420 nm = [A420 nm of the Expt (120 min)-A420 nm of the Expt



(2 min)]-[A420 nm of the Control (120 min)-A420 nm of the Control (2 min)]

Where Net A420 represents the level of oxidation of the DNA-chemical adduct. The Expt = calf thymus DNA + DNA binding agent +  $\text{KMnO}_4$ , the Control = DNA binding agent +  $\text{KMnO}_4$ .

DNA-binding compounds were generally defined as falling within the groups where the net change in absorbance between zero and various time points was  $>0.05$  or  $<-0.05$ . DNA non-binding compounds were defined as falling within the group where the net change in absorbance between zero and various time points was  $<0.05$  and  $>-0.05$  [51].

The measurement of UV absorption of compounds was conducted in the phosphate buffer by using a fixed compound concentration (250  $\mu\text{M}$ ) to which increments of the DNA stock solution was added. The solutions were allowed to incubate for 5 min before the absorption spectra were recorded [52]. The absorption spectra were recorded using Thermo Fisher Scientific Nanodrop Nd-1000 (Wilmington, USA).

#### 4.11. The fluorescent microscopy of KB3-1 cells

The KB3-1 cells were seeded in 24-well plates at 50,000 cells/mL and then allowed to adhere overnight. After, cells were treated for 24 h with compound **3.10** (1  $\mu\text{M}$ ) and doxorubicin (1  $\mu\text{M}$ ). Cells were stained with 0.2–0.5  $\mu\text{g}/\text{ml}$  of Hoechst-33342 as previously described [89]. The fluorescent microscope (Carl Zeiss, Jena, Germany), AxioImager A1 camera (at 400  $\times$  magnification), and AxioVision image analysis software Release 4.6.3.0 for Carl Zeiss microscopy (Imaging Associates Ltd., Cork, Ireland, UK) were used for KB3-1 cells examination. The Image-Pro7 software (Media Cybernetics, Rockville, Maryland, USA) was used for additional analysis of obtained photomicrographs.

#### 4.12. DNA laddering experiment

DNA extraction and gel electrophoresis were performed as described by Herrmann and others. Jurkat cells were collected by centrifugation; lysed in a lysis buffer (1% NP-40 in 20 mM EDTA, 50 mM Tris-HCl, pH 7.5; 10  $\mu\text{L}$  per 10<sup>6</sup> cells, minimum 50  $\mu\text{L}$ ). After centrifugation for 5 min at 1600 $\times$ g, the supernatant was collected and the extraction was repeated with the same amount of lysis buffer. Supernatants were brought to 1% SDS and treated for 2 h with RNase A (final concentration 5  $\mu\text{g}/\text{mL}$ ) at 56  $^\circ\text{C}$ . Then, proteinase K was added (final concentration 2.5,  $\mu\text{g}/\text{mL}$ ) and incubated for 2 h at 37  $^\circ\text{C}$ . After adding 1/2 volume of 10 M ammonium acetate, the DNA was precipitated with 2.5 vol. Ethanol, dissolved in gel loading buffer, and separated by electrophoresis in 1% agarose gels containing Ethidium bromide (at 70 V) [89].

#### 4.13. Cell cycle analysis

The cell cycle analysis and immunolabeling of cell cycle markers have been described previously. Briefly, CCRF-CEM were incubated with compounds for 24 h, then harvested, washed with cold phosphate buffered saline (PBS), fixed in cold 70% ethanol, treated with RNase (0.5 mg/mL) and stained with propidium iodide (PI) (0.1 mg/mL). The mitotic marker histone H3<sup>Ser10</sup> was detected with a specific anti-phospho-Histone H3 (Ser10) antibody (Merck Millipore). The primary antibody was diluted in blocking buffer and labeled with a secondary anti-mouse-FITC-conjugated antibody (Sigma-Aldrich). Data were acquired using FACSCalibur (Becton Dickinson) and analyzed using ModFitLT (Verity). Apoptosis was measured in logarithmic mode as the percentage of particles with PI content lower than cells in G0/G1 phase (sub-G1) of the cell cycle, and polyploidy was measured in linear mode as the percentage of particles with PI content higher than cells in the G2/M phase of the cell cycle [90].

#### 4.14. BrdU incorporation analysis (DNA synthesis)

CCRF-CEM cells were treated with the compound **3.10** at a concentration of 4.14 and 20.7  $\mu\text{M}$ . Before harvesting, 10  $\mu\text{M}$  5-bromo-2-deoxyuridine (BrdU) was added to the cells for pulse labeling for 30 min. Cells were fixed with ice-cold 70% ethanol and stored overnight. Before the analysis, cells were washed with phosphate-buffered saline (PBS) and resuspended in 2 M HCl for 30 min at room temperature to denature their DNA. Following neutralization with 0.1 M  $\text{Na}_2\text{B}_4\text{O}_7$  (Borax), cells were washed with PBS containing 0.5% Tween-20 and 1% bovine serum albumin. This was followed by staining with the primary anti-BrdU antibody (Exbio) for 30 min at room temperature in the dark followed. Then the cells were then washed with PBS and stained with the secondary antimouse-FITC antibody (Sigma-Aldrich, USA). Then, cells were then rewashed again with PBS and incubated with propidium iodide (0.05 mg/mL, Sigma-Aldrich, USA) and RNase A (1 mg/mL, Sigma-Aldrich, USA) for 1 h at room temperature in the dark and afterward analyzed by flow cytometry using a 488 nm single beam laser (FACS Calibur; Becton Dickinson) [90].

#### 4.15. BrdU incorporation analysis (RNA synthesis)

CCRF-CEM cells were cultured and treated as described above. This was followed by pulse labeling with 1 mM BrU for 30 min before harvesting. Cells were then fixed in 1% buffered paraformaldehyde with 0.05% of NP-40 at room temperature for 15 min and then stored at 4  $^\circ\text{C}$  overnight. Before measurement, they were washed in PBS with 1% glycine, washed again in PBS and stained with primary anti-BrdU antibody cross-reacting to BrU (Exbio) for 30 min at room temperature in the dark. After another washing in PBS, cells were stained with secondary antimouse-FITC antibody (Sigma). After staining, the cells were washed with PBS and fixed with 1% paraformaldehyde-buffered with PBS with 0.05% of NP-40 for 1 h. The cells were washed with PBS, incubated with propidium iodide (0.05 mg/mL, Sigma-Aldrich, USA) and RNase A (1 mg/mL, Sigma-Aldrich, USA) for 1 h at room temperature in the dark and finally analyzed by flow cytometry using a 488 nm single beam laser (FACS Calibur; Becton Dickinson) [90].

#### 4.16. Flow cytometry assessment of annexin V and propidium iodide binding

The apoptosis induction by the tested compounds was assessed by the exposure of phosphatidylserine on the cell membrane, to which fluorescein isothiocyanate (FITC)-labeled annexin V binds with high affinity in the presence of  $\text{Ca}^{2+}$  ions. The FITC Annexin V Apoptosis Detection Kit II (BD Pharmingen, San Diego, CA, USA) and a flow cytometer (BD FACSCanto II, BD Biosciences Systems, San Jose, CA, USA) were used for this detection. The assay was performed according to the manufacturer's instructions. Breast cancer cells (MDA-MB-231) were incubated for 24 h (37  $^\circ\text{C}$ , 5%  $\text{CO}_2$ , 90–95% humidity) with the tested compounds (**3.10** and **3.4**) at concentrations of 5  $\mu\text{M}$  and 10  $\mu\text{M}$ . Flow cytometer calibration was performed by preparing two controls - a positive and negative control. The positive control were cells in which apoptosis was induced using 2  $\mu\text{L}$  of 3% formaldehyde in buffer and placing them on ice for 30 min. In contrast, the negative control was represented by cells that were not treated with any of the proapoptotic agents. First, in cells treated with the tested compounds as well as the controls, the medium was removed and the cells were washed twice with cold PBS. Subsequently, cells were resuspended in Binding Buffer included in the kit at a concentration of  $1 \times 10^6$  cells/mL. From each sample, 100  $\mu\text{L}$  of cell suspension was taken and transferred to test tubes to which 5  $\mu\text{L}$  each of FITC Annexin V and propidium iodide (PI) were then added. The contents of the test tubes were gently vortexed and incubated for 15 min at room temperature, protected from light. After the required time, the contents of the test tubes were made up to 500  $\mu\text{L}$  with Binding Buffer and immediately analyzed in a flow cytometer

(10,000 events measured). After flow cytometer readout, results were analyzed using FACSDiva software (BD Biosciences Systems, San Jose, CA, USA). The equipment was calibrated with BD Cytometer Setup and Tracking Beads (BD Biosciences, San Diego, CA, USA) [61].

#### 4.17. Determination of mitochondrial membrane potential

Disruption of the MMP was assessed using the lipophilic cationic probe 5,5,6,6-tetrachloro-1,1,3,3-tetraethylbenzimidazolcarbocyanine iodide (JC-1 MitoScreen kit; BD Biosciences) as described previously [92]. Briefly, unfixed cells were washed and resuspended in PBS supplemented with JC-1. Cells were then incubated for 15 min at room temperature (RT) in the dark, washed, and resuspended in PBS for immediate BD FACSCanto II flow cytometry analysis. The percentage of cells with disrupted MMP was calculated in the FACSDiva software (both from BD Biosciences Systems, San Jose, CA, USA).

#### 4.18. Caspase 3/7, 8 and 9 activity assay

Activation of the caspase cascade occurs as a result of the initiation of the apoptotic process in the cell and is induced by the cytotoxic activity of the compound. In this regard, assessment of initiator (caspase 8 and 9) and executioner (caspase 3 and 7) caspases activity was performed using FAM-FLICA® Caspase Assays kits (all from ImmunoChemistry Technologies, Bloomington, MN, USA) according to the manufacturer's instructions. After 24 h incubation of MDA-MB-231 breast cancer cells with the tested compounds (**3.10** and **3.4**) at concentrations of 5  $\mu$ M and 10  $\mu$ M, cells were collected, washed twice with cold PBS, and resuspended in Apoptosis Wash Buffer to a final concentration of  $5 \times 10^5$  cells/mL. In the next step, 290  $\mu$ L each of cell suspension was taken and transferred into tubes. Then, 10  $\mu$ L each of FLICA solution diluted immediately before use (1:5 v/v, using PBS) was added to the cells, mixed by pipetting, and incubated in the dark for 1 h at 37 °C. After this time, cells were washed twice with 2 mL Apoptosis Wash Buffer, centrifuged, and resuspended in 300  $\mu$ L of the buffer. Thus prepared samples were immediately analyzed using a BD FACSCanto II flow cytometer (10,000 events) with FACSDiva software (both from BD Biosciences Systems, San Jose, CA, USA). The equipment calibration was performed using BD Cytometer Setup and Tracking Beads (BD Biosciences, San Diego, CA, USA) [61].

#### 4.19. Western blot analysis

To check does compound **3.10** can cause a stress of Endoplasmatic reticulum as a part of its mechanism of action Western blot analysis of corresponding proteins (BIP, PDI, Calnexin) was performed. First, KB-3 cells were seeded in a 6-well plate ( $5 \times 10^5$  cells/mL/well) and after 24 h recovery, treated with the drug in different concentrations and left to growth for next 3 h or 24 h. After 3 and 24 h drug expose cells were harvested, proteins were isolated resolved by SDS/PAGE, and transferred onto a PVDF membrane for Western blotting (Sigma Aldrich) as described previously. The following antibodies were used: BIP (#3177, Cell Signaling Technology, USA), PDI (#2446, Cell Signaling Technology, USA), Calnexin (#2433, Cell Signaling Technology, USA) and  $\beta$ -actin (A5441, Sigma Aldrich). All primary antibodies were used in 1:1000 dilutions in 3% BSA and 5%-Na<sub>3</sub>N-containing Tris-buffered saline. Additionally, peroxidase-labeled secondary antibodies antimouse (#7076 Cell Signaling Technology, USA) and anti-rabbit (A0168, Sigma-Aldrich) were used at working dilutions of 1:10000 [91].

#### 4.20. In vivo toxicity study of **3.10**

**Animals.** Studies of the acute cytotoxic activity of **3.10** *in vivo* was conducted in 2022 at the animal facility of the Institute of Cell Biology, NAS of Ukraine (Lviv, Ukraine). 14 adult male C57BL/6 mice with 23 g average weight were kept under standard vivarium conditions with

constant access to the full feed and drinking water. Animals were divided into 3 groups. Mice from the 2<sup>nd</sup> group were administered intraperitoneally with Doxorubicin (Dox, n = 4) at a dose of 6.6 mg/kg every 48 h from the 1<sup>st</sup> to the 5<sup>th</sup> day of the experiment (3 injections). Doxorubicin was used as a positive control and its cumulative dose was 20 mg/kg. Animals from the 3<sup>rd</sup> group were injected intraperitoneally (*i. p.*) with compound **3.10** (n = 6) at a dose of 6.6 mg/kg every 48 h three times (the total dose also was 20 mg/kg). Mice from 1<sup>st</sup> control-vehicle group were treated with equivalent volume of saline solution (0.9% sodium chloride solution) in a similar mode.

Mice were monitored daily for survival and body weight. Survival data are plotted on a Kaplan-Meier curves. Graphs of changes in the weight of animals during the experiment were drawn. The animals were sacrificed on the 22<sup>nd</sup> day of the experiment (that is, the 22<sup>nd</sup> day after the 1st and the 17<sup>th</sup> day after the last injection of the compounds). Vital organs (namely the heart, liver, spleen, kidneys, lungs) were isolated and weighed. Then the organ-to-body weight indices were calculated according to the following formula: (organ weight  $\times$  100)/body weight.

**Blood sampling.** Blood was collected from the retro-orbital sinus of mice. For blood sampling animal was scruffed with thumb and forefinger of the non-dominant hand and the skin around the eye was pulled taut. Then capillary tube/pipette was inserted into the medial canthus of the eye (30-degree angle to the nose). The capillary tube/pipette was gently removed and wiped the mouse's eye with sterile cotton after the required volume of blood was collected. For hematological analysis, blood samples (100  $\mu$ L) were collected from mice via a retro-orbital bleed in microtubes containing 5  $\mu$ L of 10% ethylenediaminetetraacetic acid disodium salt solution (Na<sub>2</sub>-EDTA solution) as an anticoagulant.

**Hematological analysis.** Hematological profile changes were studied by 5-Part automated hematology analyzer DF-51 (DYMIND Biotechnology Co., Ltd, Shenzhen, China) using high quality hematology analyzer reagents (Dymind Biotechnology Co., Ltd, Shenzhen, China) according to manufacturer's instructions. Blood for the study was collected on the 22nd day after the first injection of the studied compound.

All *in vivo* experiments were conducted in accordance with the international principles of the European Convention for protection of vertebrate animals under a control of the Bio-Ethics Committee of the above-mentioned institution (Protocol N 4/2016 from 5.06.2016 of the BioEthics Committee at the Institute of Cell Biology, NAS of Ukraine).

**Statistical analysis.** The results were analyzed with GraphPad Prism 6 (GraphPad Software, USA), and presented as a mean (M)  $\pm$  standard deviation (SD) of 3 parallels. Statistical evaluation was performed using a two-way ANOVA analysis followed by Tukey's multiple comparisons test. The P-value of  $\leq 0.05$  was considered as statistically significant [92].

#### 4.21. Compliance with ethical standards

All experiments with isolated human lymphocytes from peripheral blood of adult healthy donor and patients with acute and chronic leukemia were approved by Ethics Committee of the Institute of Cell Biology of National Academy of Sciences of Ukraine (protocols No 2 from January 27, 2019 and No 2 from October 7, 2020) and with written consent of donor.

All *in vivo* experiments were conducted in accordance with the international principles of the European Convention for protection of vertebrate animals under a control of the Bio-Ethics Committee of the above-mentioned institution (Protocol N 4/2016 from 5.06.2016 of the BioEthics Committee at the Institute of Cell Biology, NAS of Ukraine).

#### Author contributions

Conceptualization, Roman Lesyk, Andrii Lozynskiy and Rostyslav Stoika; methodology, Andrii Lozynskiy, Dmytro Khylyuk, Anna

Bielawska, Krzysztof Bielawski, and Andrzej Gzella; software, Andriy Karkhut, Dmytro Khylyuk; validation, Olga Klyuchivska, Nataliya Kashchak, Nazar Manko, Zvenyslava Maslyak, Julia Senkiv; formal analysis, Svyatoslav Polovkovych; investigation, Andrii Lozynskiy, Iryna Ivasechko, Piotr Roszczenko, Yuliia Kozak, Danylo Lesyk, Olga Szweczyk, Marian Hajdych, and Nataliya Finiuk; resources, Krzysztof Bielawski, Roman Lesyk and Rostyslav Stoika; data curation, Sona Gurska; writing—original draft preparation, Andrii Lozynskiy, Iryna Ivasechko and Roman Lesyk; writing—review and editing, Krzysztof Bielawski, Anna Bielawska, Nataliya Finiuk, Roman Lesyk and Rostyslav Stoika; visualization, Dmytro Khylyuk, Olexandr Karpenko, Robert Czarnomysy, Petr Dzubak, Andriy Kozytyskiy; supervision, Roman Lesyk; project administration, Roman Lesyk and Rostyslav Stoika. All authors have read and agreed to the published version of the manuscript.

## Declaration of competing interest

The authors declare that they have no known competing financial interests or personal relationships that could have appeared to influence the work reported in this paper.

## Data availability

Data will be made available on request.

## Acknowledgement

The research leading to these results has received funding from the Polish National Agency for Academic Exchange (NAWA) under the “Strategic Partnerships” program (Grant agreement no. BPI/PST/2021/1/00002/U/00001), the Ministry of Health of Ukraine, under the project number 0121U100690, and the National Research Foundation of Ukraine, under the project number:2020.02/0035. This work was also supported by infrastructural projects (CZ-OPENSURE – LM2023052) and National Institute for Cancer Research (Programme EXCELES, ID Project No. LX22NPO5102) - Funded by the European Union - Next Generation EU. We are grateful to G. Morris from Drug Synthesis and Chemistry Branch, National Cancer Institute, Bethesda, MD, USA, for *in vitro* evaluation of anticancer activity.

The authors would like to thank all the brave defenders of Ukraine who made the finalization of this article possible.

## Appendix A. Supplementary data

Supplementary data to this article can be found online at <https://doi.org/10.1016/j.ejmech.2023.115304>.

## References

- [1] H.P. Song, S.Q. Wu, L.W. Qi, F. Long, L.F. Jiang, K. Liu, H. Zeng, Z.M. Xu, P. Li, H. Yang, A strategy for screening active lead compounds and functional compound combinations from herbal medicines based on pharmacophore filtering and knockout/knockin chromatography, *J. Chromatogr. A* 1456 (2016) 176–186, <https://doi.org/10.1016/j.chroma.2016.06.009>.
- [2] A.Y. Khormi, T.A. Farghaly, A. Bayazeed, Y.O. Al-Ghamdi, H.G. Abdulwahab, M. R. Shaaban, Novel thiazole derivatives incorporating phenyl sulphonyl moiety as potent BRAFV600E kinase inhibitors targeting melanoma, *RSC Adv.* 12 (2022) 27355–27369, <https://doi.org/10.1039/D2RA03624J>.
- [3] E.M.H. Abbas, T.A. Farghaly, R. Sabour, M.R. Shaaban, Z.A. Abdallah, Design, synthesis, cytotoxicity, and molecular docking studies of novel thiazolyl-hydrazone derivatives as histone lysine acetyl-transferase inhibitors and apoptosis inducers, *Arch. Pharm.* (2022) 355, <https://doi.org/10.1002/ardp.202200076>.
- [4] A.M. Alsaedi, T.A. Farghaly, M.R. Shaaban, Fluorinated azole anticancer drugs: synthesis, elaborated structure elucidation and docking studies, *Arab. J. Chem.* 15 (5) (2022) 1878–5352, <https://doi.org/10.1016/j.arabjc.2022.103782>.
- [5] A. Kryshchysyn, O. Roman, A. Lozynskiy, R. Lesyk, Thiopyrano[2,3-*d*]thiazoles as new efficient scaffolds in medicinal chemistry, *Sci. Pharm.* 86 (2) (2018) 26, <https://doi.org/10.3390/scipharm86020026>.
- [6] R. Lesyk, B. Zimenkovsky, D. Atamanyuk, F. Jensen, K. Kieć-Kononowicz, A. Gzella, Anticancer thiopyrano[2,3-*d*][1,3]thiazol-2-ones with norbornane moiety. Synthesis, cytotoxicity, physico-chemical properties, and computational studies, *Bioorg. Med. Chem.* 14 (15) (2006) 5230–5240, <https://doi.org/10.1016/j.bmc.2006.03.053>.
- [7] D. Atamanyuk, B. Zimenkovsky, V. Atamanyuk, R. Lesyk, 5-Ethoxymethylidene-4-thioxo-2-thiazolidinone as versatile building block for novel biorelevant small molecules with thiopyrano[2,3-*d*][1,3]thiazole core, *Synth. Commun.* 44 (2) (2014) 237–244, <https://doi.org/10.1080/00397911.2013.800552>.
- [8] A.V. Lozynskiy, D.V. Kaminsky, K.B. Romanchyshyn, N.G. Semenciv, V. V. Ogurtsov, I.O. Nektegayev, R.B. Lesyk, Screening of antioxidant and anti-inflammatory activities among thiopyrano[2,3-*d*]thiazoles, *Biopolym. Cell* 31 (2) (2015) 131–137, <https://doi.org/10.7124/bc.0008D8>.
- [9] A. Lozynskiy, S. Golota, B. Zimenkovsky, D. Atamanyuk, A. Gzella, R. Lesyk, Synthesis, anticancer and antiviral activities of novel thiopyrano[2,3-*d*]thiazole-6-carbaldehydes, *Phosphorus Sulfur Silicon Relat. Elements* 191 (9) (2016) 1245–1249, <https://doi.org/10.1080/10426507.2016.1166108>.
- [10] N. Zelisko, D. Atamanyuk, O. Vasylenko, P. Grellier, R. Lesyk, Synthesis and antitrypanosomal activity of new 6,6,7-trisubstituted thiopyrano[2,3-*d*][1,3]thiazoles, *Bioorg. Med. Chem. Lett.* 22 (23) (2012) 7071–7074, <https://doi.org/10.1016/j.bmcl.2012.09.091>.
- [11] N.H. Metwally, A simple green synthesis of (Z)-5-arylmethylene-4-thioxothiazolidines and thiopyrano[2,3-*d*]thiazolidine-2-thiones in PEG-400 under catalyst-free conditions, *J. Sulphur Chem.* 35 (5) (2014) 528–537, <https://doi.org/10.1080/17415993.2014.933341>.
- [12] F.M. Abdelrazek, Z.E. Kandeel, K.M. Himiy, M.H. Elnagdi, Substituted acrylonitriles in heterocyclic synthesis. The reaction of  $\alpha$ -substituted  $\beta$ -(2-furyl)-acrylonitriles with some active-methylene heterocycles, *Synthesis* 4 (1985) 432–434, <https://doi.org/10.1055/s-1985-31232>.
- [13] A. Lozynskiy, I. Yushyn, Y. Shepeta, O. Karpenko, A.K. Gzella, R. Lesyk, Synthesis and structure elucidation of thiopyrano[2,3-*d*]thiazole-6-carbonitriles as adducts of Michael reaction, *J. Mol. Struct.* 1256 (2022), 132574 <https://doi.org/10.1016/j.molstruc.2022.132574>.
- [14] A. Lozynskiy, B. Zimenkovsky, I. Yushyn, D. Kaminsky, O. Karpenko, A.K. Gzella, R. Lesyk, Synthesis of new structurally diverse thiazolidinone-derived compounds based on reaction of isorhodanine with ortho-substituted aldehydes,  $\alpha$ -keto- and  $\beta$ -aroylacrylic acids, *J. Mol. Struct.* 1217 (2020), 128448, <https://doi.org/10.1016/j.molstruc.2020.128448>.
- [15] D. Majiene, J. Kuseliuskite, A. Stimbirys, A. Jekabsonė, Comparison of the effect of native 1, 4-naphthoquinones plumbagin, menadione, and lawsone on viability, redox status, and mitochondrial functions of C6 glioblastoma cells, *Nutrients* 11 (6) (2019) 1294, <https://doi.org/10.3390/nu11061294>.
- [16] N.G. Deniz, C. Ibis, Z. Gokmen, M. Stasevych, V. Novikov, O. Komarovska-Porokhnyavets, M. Ozyurek, K. Guclu, D. Karakas, E. Ulukay, Design, synthesis, biological evaluation, and antioxidant and cytotoxic activity of heteroatom-substituted 1, 4-naphtho- and benzoquinones, *Chem. Pharm. Bull.* 63 (12) (2015) 1029–1039, <https://doi.org/10.1248/cpb.c15-00607>.
- [17] Milackova, M.S. Prnova, M. Majekova, R. Sotnikova, M. Stasko, L. Kovacicova, S. Banerjee, M. Veverka, M. Stefek, 2-Chloro-1,4-naphthoquinone derivative of quercetin as an inhibitor of aldose reductase and anti-inflammatory agent, *J. Enzym. Inhib. Med. Chem.* 30 (1) (2015) 107–113, <https://doi.org/10.3109/14756366.2014.892935>.
- [18] C.E. Pereyra, R.F. Dantas, S.B. Ferreira, L.P. Gomes, F.P. Silva Jr., The diverse mechanisms and anticancer potential of naphthoquinones, *Cancer Cell Int.* 19 (1) (2019) 1–20, <https://doi.org/10.1186/s12935-019-0925-8>.
- [19] V.K. Tandon, S. Kumar, Recent development on naphthoquinone derivatives and their therapeutic applications as anticancer agents, *Expert Opin. Ther. Pat.* 23 (9) (2013) 1087–1108, <https://doi.org/10.1517/13543776.2013.798303>.
- [20] N. Kretschmer, B. Rinner, A.J. A. Deutsch, B. Lohberger, H. Knausz, O. Kunert, M. Blunder, H. Boechzelt, H. Schaidler, R. Bauer, Naphthoquinones from *Onosma paniculata* induce cell-cycle arrest and apoptosis in melanoma cells, *J. Nat. Prod.* 75 (5) (2012) 865–869, <https://doi.org/10.1021/np2006499>.
- [21] E. Leyva, L.I. López, R.F.G. de la Cruz, C.G. Espinosa-González, Synthesis and studies of the antifungal activity of 2-anilino-/2,3-dianilino-/2-phenoxy- and 2,3-diphenoxy-1,4-naphthoquinones, *Res. Chem. Intermed.* 43 (2017) 1813–1827, <https://doi.org/10.1007/s11164-016-2732-3>.
- [22] M.H. Khraiwesh, C.M. Lee, Y. Brandy, E.S. Akinboye, S. Berhe, G. Gittens, M. M. Abbas, F.R. Ampy, M. Ashraf, O. Bakare, Antitrypanosomal activities and cytotoxicity of some novel imidosubstituted 1,4-naphthoquinone derivatives, *Arch. Pharm. Res. (Seoul)* 35 (1) (2012) 27–33, <https://doi.org/10.1007/s12272-012-0103-1>.
- [23] C. dos S Moreira, T.B. Santos, R.H. Freitas, P.A. Pacheco, D.R. da Rocha, Juglone: a versatile natural platform for obtaining new bioactive compounds, *Curr. Top. Med. Chem.* 21 (22) (2021) 2018–2045, <https://doi.org/10.2174/1568026621666210804121054>.
- [24] Y.T. Tang, Y. Li, P. Chu, X.D. Ma, Z.Y. Tang, Z.L. Sun, Molecular biological mechanism of action in cancer therapies: juglone and its derivatives, the future of development, *Biomed. Pharmacother.* 148 (2022), 112785, <https://doi.org/10.1016/j.biopha.2022.112785>.
- [25] T. Ahmad, Y.J. Suzuki, Juglone in oxidative stress and cell signaling, *Antioxidants* 8 (4) (2019) 91, <https://doi.org/10.3390/antiox8040091>.
- [26] M. Strugstad, S. Despotovski, A summary of extraction, synthesis, properties, and potential uses of juglone: a literature review, *J. Ecosyst. Manag.* 13 (3) (2012) 1–16, <https://doi.org/10.22230/jem.2012v13n3a119>.
- [27] A. Medic, T. Zamljen, A. Slatnar, M. Hudina, R. Verberic, Is juglone the only naphthoquinone in *Juglans regia* L. with allelopathic effects? *Agriculture* 11 (8) (2021) 784, <https://doi.org/10.3390/agriculture11080784>.



- [28] M.T. Paulsen, M. Ljungman, The natural toxin juglone causes degradation of p53 and induces rapid H2AX phosphorylation and cell death in human fibroblasts, *Toxicol. Appl. Pharmacol.* 209 (1) (2005) 1–9, <https://doi.org/10.1016/j.taap.2005.03.005>.
- [29] C. Wu, Y. Ha, Y. Zou, X. Liao, S. Zhang, X. Zhang, R. Li, J. Xing, W. Jie, J. Guo, J. Li, Z. Shen, Pathologic role of peptidyl-prolyl isomerase Pin1 in pulmonary artery remodeling, *Am. J. Transl. Res.* 13 (10) (2021) 11162–11177.
- [30] Y.Y. Zhang, Z.J. Ni, E. Elam, F. Zhang, K. Thakur, S. Wang, Z. Jian-Guo, Z.J. Wei, Juglone, a novel activator of ferroptosis, induces cell death in endometrial carcinoma Ishikawa cells, *Food Funct.* 12 (11) (2021) 4947–4959, <https://doi.org/10.1039/D1FO00790D>.
- [31] Y.Y. Zhang, F. Zhang, Y.S. Zhang, K. Thakur, J.G. Zhang, Y. Liu, K. Huan, Z.J. Wei, Mechanism of juglone-induced cell cycle arrest and apoptosis in Ishikawa human endometrial cancer cells, *J. Agric. Food Chem.* 67 (26) (2019) 7378–7389, <https://doi.org/10.1021/acs.jafc.9b02759>.
- [32] S. Calabrò, K. Alzoubi, R. Bissinger, K. Jilani, C. Faggio, F. Lang, Enhanced eryptosis following juglone exposure, *Basic Clin. Pharmacol. Toxicol.* 116 (6) (2015) 460–467, <https://doi.org/10.1111/bcpt.12340>.
- [33] W. Zhang, A. Liu, Y. Li, X. Zhao, S. Lv, W. Zhu, Y. Jin, Anticancer activity and mechanism of juglone on human cervical carcinoma HeLa cells, *Can. J. Physiol. Pharmacol.* 90 (11) (2012) 1553–1558, <https://doi.org/10.1139/y2012-134>.
- [34] A. Lozynski, J. Senkiv, I. Ivasechko, N. Finiuk, O. Klyuchivska, N. Kashchak, D. Lesyk, A. Karkhut, S. Polovkovych, O. Levytska, O. Karpenko, A. Boshkayeva, G. Sayakova, A. Gzella, R. Stoika, R. Lesyk, 1,4-Naphthoquinone motif in the synthesis of new thiopyrano[2,3-d]thiazoles as potential biologically active compounds, *Molecules* 27 (21) (2022) 7575, <https://doi.org/10.3390/molecules27217575>.
- [35] A. Lozynski, B. Zimenkovsky, I. Nektegayev, R. Lesyk, Arylidene pyruvic acids motif in the synthesis of new thiopyrano[2,3-d]thiazoles as potential biologically active compounds, *Heterocycl. Commun.* 21 (1) (2015) 55–59, <https://doi.org/10.1515/hc-2014-0204>.
- [36] M.C. Carreño, A. Urbano, C. Di Vitta, Enantioselective Diels-Alder approach to C-3-oxygenated angucyclinones from (SS)-2-(p-tolylsulfanyl)-1,4-naphthoquinone, *Chem. Eur. J.* 6 (5) (2000) 906–913, [https://doi.org/10.1002/\(SICI\)1521-3765\(20000303\)6:5<906::AID-CHEM906>3.0.CO;2-G](https://doi.org/10.1002/(SICI)1521-3765(20000303)6:5<906::AID-CHEM906>3.0.CO;2-G).
- [37] K.B.S. Magar, L. Xia, Y.R. Lee, Organocatalyzed benzannulation for the construction of diverse anthraquinones and tetracenediones, *Chem. Commun. (J. Chem. Soc. Sect. D)* 51 (41) (2015) 8592–8595, <https://doi.org/10.1039/C5CC00623F>.
- [38] A.F. Abdassalam, N.G. Deniz, C. Sayil, M. Ozyurek, E.A. Yesil, H. Salihoglu, Synthesis of new regioisomers of 5-nitro-1,4-naphthoquinone, evaluation of antioxidant and catalase inhibition activities, *Acta Chim. Slov.* 69 (1) (2022) 187–199, <https://doi.org/10.17344/actsi.2021.7123>.
- [39] A.L. Spek, Structure validation in chemical crystallography, *Acta Crystallogr.* 65 (2009) 148–155, <https://doi.org/10.1107/S0907444490804362X>.
- [40] F.H. Allen, O. Kennard, D.G. Watson, L. Brammer, A.G. Orpen, R. Taylor, Tables of bond lengths determined by X-ray and neutron diffraction. Part 1. Bond lengths in organic compounds, *J. Chem. Soc. Perkin Trans. 2* (12) (1987) S1–S19, <https://doi.org/10.1039/P29870000051>.
- [41] M.R. Boyd, K.D. Paull, Some practical considerations and applications of the national cancer Institute *in vitro* anticancer drug discovery screen, *Drug Dev. Res.* 34 (2) (1995) 91–109, <https://doi.org/10.1002/ddr.430340203>.
- [42] R.H. Shoemaker, The NCI60 human tumour cell line anticancer drug screen, *Nat. Rev. Cancer* 6 (10) (2006) 813–823, <https://doi.org/10.1038/nrc1951>.
- [43] M.R. Boyd, The NCI *in vitro* anticancer drug discovery (60-cell) screen, in: B. A. Teicher (Ed.), *Anticancer Drug Development Guide*. Cancer Drug Discov. Dev., Humana Press, Totowa, New Jersey, 2004, pp. 41–61, [https://doi.org/10.1007/978-1-59259-739-0\\_3](https://doi.org/10.1007/978-1-59259-739-0_3).
- [44] W.W. Van Osdol, T.G. Myers, K.D. Paull, K.W. Kohn, J.N. Weinstein, Use of the Kohn self-organizing map to study the mechanisms of action of chemotherapeutic agents, *J. Natl. Cancer Inst.* 86 (24) (1994) 1853–1859, <https://doi.org/10.1093/jnci/86.24.1853>.
- [45] M.Y. Son, C.X. Deng, J.H. Hoelijmarkers, V.I. Rebel, P. Hasty, A mechanism for 1,4-benzoquinone-induced genotoxicity, *Oncotarget* 7 (29) (2016) 46433–46447, <https://doi.org/10.18632/oncotarget.10184>.
- [46] Z. Zuo, X. Liu, X. Qian, T. Zeng, N. Sang, H. Liu, Y. Zhou, L. Tao, X. Zhou, N. Su, Y. Yu, Q. Chen, Y. Luo, Y. Zhao, Bifunctional naphtho[2,3-d][1,2,3]triazole-4,9-dione compounds exhibit antitumor effects *in vitro* and *in vivo* by inhibiting dihydroorotate dehydrogenase and inducing reactive oxygen species production, *J. Med. Chem.* 63 (14) (2020) 7633–7652, <https://doi.org/10.1021/acs.jmedchem.0c00512>.
- [47] F. Gellibert, J. Woolven, M.H. Fouchet, N. Mathews, H. Goodland, V. Lovegrove, A. Laroze, V.-L. Nguyen, S. Sautet, R. Wang, C. Janson, W. Smith, G. Krysa, V. Boullay, A.-C. de Gouville, S. Huet, D. Hartley, Identification of 1,5-naphthyridine derivatives as a novel series of potent and selective TGF- $\beta$  type I receptor inhibitors, *J. Med. Chem.* 47 (18) (2004) 4494–4506, <https://doi.org/10.1021/jm0400247>.
- [48] Y. Filyak, O. Filyak, S. Souchelnyskiy, R. Stoika, Doxorubicin inhibits TGF- $\beta$  signaling in human lung carcinoma A549 cells, *Eur. J. Pharmacol.* 590 (1–3) (2008) 67–73, <https://doi.org/10.1016/j.ejphar.2008.05.030>.
- [49] R. Palchadhuri, P.J. Hergenrother, DNA as a target for anticancer compounds: methods to determine the mode of binding and the mechanism of action, *Curr. Opin. Biotechnol.* 18 (6) (2007) 497–503, <https://doi.org/10.1016/j.copbio.2007.09.006>.
- [50] R. Martínez, L. Chacón-García, The search of DNA-intercalators as antitumoral drugs: what it worked and what did not work, *Curr. Med. Chem.* 12 (2) (2005) 127–151, <https://doi.org/10.2174/0929867053363414>.
- [51] A. Garas, E. Webb, V. Pillay, D. MacPhee, W. Denny, H. Zeller, R. Cotton, A novel and simple method of screening compounds for interaction with DNA: a validation study, *Mutat. Res., Genet. Toxicol. Environ. Mutagen.* 678 (1) (2009) 20–29, <https://doi.org/10.1016/j.mrgentox.2009.06.005>.
- [52] M. Sirajuddin, S. Ali, A. Badshah, Drug–DNA interactions and their study by UV–Visible, fluorescence spectroscopies and cyclic voltametry, *J. Photochem. Photobiol., A* 124 (2013) 1–19, <https://doi.org/10.1016/j.jphotobiol.2013.03.013>.
- [53] G. Saibaba, B. Janani, R. Mohamed Asik, D. Rajesh, G. Pugalenth, J. Angayarkanni, G. Archunan, Natural lovastatin (NL) as an anticancer agent: docking and experimental studies, *ICTMI* 2017 (2019) 115–135, [https://doi.org/10.1007/978-981-13-1477-3\\_10](https://doi.org/10.1007/978-981-13-1477-3_10).
- [54] J. Bai, Y. Li, G. Zhang, Cell cycle regulation and anticancer drug discovery, *Cancer Biol. Med.* 14 (4) (2017) 348–362, <https://doi.org/10.20892/j.issn.2095-3941.2017.0033>.
- [55] Z. Darzynkiewicz, G. Juan, DNA content measurement for DNA ploidy and cell cycle analysis, *Curr. Protoc. Cytom* 1 (1997) 7, <https://doi.org/10.1002/0471142956.cy0705s00>, 5.1-7.5.24.
- [56] H. Yoshida, T. Matsui, A. Yamamoto, T. Okada, K. Mori, XBP1 mRNA is induced by ATF6 and spliced by IRE1 in response to ER stress to produce a highly active transcription factor, *Cell* 107 (7) (2001) 881–891, [https://doi.org/10.1016/S0092-8674\(01\)00611-0](https://doi.org/10.1016/S0092-8674(01)00611-0).
- [57] A. Hetz, F.R. Papa, The unfolded protein response and cell fate control, *Mol. Cell* 69 (2) (2018) 169–181, <https://doi.org/10.1016/j.molcel.2017.06.017>.
- [58] R. Singh, A. Letai, K. Sarosiek, Regulation of apoptosis in health and disease: the balancing act of BCL-2 family proteins, *Nat. Rev. Mol. Cell Biol.* 20 (2019) 175–193, <https://doi.org/10.1038/s41580-018-0089-8>.
- [59] A. Urbani, E. Prodocimi, A. Carrer, V. Checchetto, I. Szabó, Mitochondrial ion channels of the inner membrane and their regulation in cell death signaling, *Front. Cell Dev. Biol.* 8 (2021), 620081, <https://doi.org/10.3389/fcell.2020.620081>.
- [60] R. Czarnomysy, A. Muszyńska, J. Rok, Z. Rzepka, K. Bielawski, Mechanism of anticancer action of novel imidazole platinum(II) complex conjugated with G2 PAMAM-OH dendrimer in breast cancer cells, *Int. J. Mol. Sci.* 22 (11) (2021) 5581, <https://doi.org/10.3390/ijms22115581>.
- [61] A. Radomska, R. Czarnomysy, A. Szymanowska, D. Radomski, E. Domínguez-Álvarez, A. Bielawska, K. Bielawski, Novel selenoesters as a potential tool in triple-negative breast cancer treatment, *Cancers* 14 (17) (2022) 4304, <https://doi.org/10.3390/cancers14174304>.
- [62] L.A. Biondo, L.S. Silveira, A.A. de Souza Teixeira, J.C. Rosa Neto, White adipose tissue and cancer: impacts of doxorubicin and potential Co-therapies, *2020, Immunometabolism* 2 (4) (2020), e200030, <https://doi.org/10.20900/immunometab20200030>.
- [63] A.E. Hienrich, K.A. Bolam, S. Mijwel, J.A.L. Jenson, A.D.R. Huitema, O. Kranenburg, E. van der Wall, H. Rundqvist, Y. Wengstrom, A.M. May, Doxorubicin-induced skeletal muscle atrophy: elucidating the underlying molecular pathways, *Acta Physiol.* 229 (2) (2020), e13400, <https://doi.org/10.1111/apha.13400>.
- [64] T. Chen, H.M. Shen, Z.Y. Deng, Z.Z. Yang, R.L. Zhao, L. Wang, Z.P. Feng, C. Liu, W. H. Li, Z.J. Liu, A herbal formula, SYKT, reverses doxorubicin-induced myelosuppression and cardiotoxicity by inhibiting ROS-mediated apoptosis, *Mol. Med. Rep.* 15 (4) (2017) 2057–2066, <https://doi.org/10.3892/mmr.2017.6272>.
- [65] L. Repetto, CIPOMO investigators, Incidence and clinical impact of chemotherapy induced myelotoxicity in cancer patients: an observational retrospective survey, *Crit. Rev. Oncol. Hematol.* 72 (2) (2009) 170–179, <https://doi.org/10.1016/j.critrevonc.2009.03.004>.
- [66] Z. Nurgalieva, C.C. Liu, X.L. Du, Chemotherapy use and risk of bone marrow suppression in a large population-based cohort of older women with breast and ovarian cancer, *Med. Oncol.* 28 (3) (2011) 716–725, <https://doi.org/10.1007/s12032-010-9512-5>.
- [67] A. Daniel, J. Crawford, Myelotoxicity from chemotherapy, *Semin. Oncol.* 33 (1) (2006) 74–85, <https://doi.org/10.1053/j.seminoncol.2005.11.003>.
- [68] S.E. Owumi, S.O. Nwozo, U.O. Arunsi, A.K. Oyelere, O.A. Odunola, Co-administration of Luteolin mitigated toxicity in rats' lungs associated with doxorubicin treatment, *Toxicol. Appl. Pharmacol.* 411 (2021), 115380, <https://doi.org/10.1016/j.taap.2020.115380>.
- [69] A. Shaldoum, A.F. El-Kott, M.M.A. Ouda, E.M. Abd-Ella, Immunomodulatory effects of bee pollen on doxorubicin-induced bone marrow/spleen immunosuppression in rat, *J. Food Biochem.* 45 (6) (2021), e13747, <https://doi.org/10.1111/jfbc.13747>.
- [70] A.E. Nugroho, A. Hermawan, K. Nastiti, S. Suven, P. Elisa, T. Hadibarata, E. Meiyanto, Immunomodulatory effects of hexane insoluble fraction of *Ficus septica* Burm. F. in doxorubicin-treated rats, *Asian Pac. J. Cancer Prev. APJCP* 13 (11) (2012) 5785–5790, <https://doi.org/10.7314/apjcp.2012.13.11.5785>.
- [71] D.J.M. Lamas, M.B. Nicoud, H.A. Sterle, E. Carabajal, F. Tesan, J.C. Perazzo, G. A. Cremaschi, E.S. Rivera, V.A. Medina, Selective cytoprotective effect of histamine on doxorubicin-induced hepatic and cardiac toxicity in animal models, *Cell Death Dis.* 1 (2015), 15059, <https://doi.org/10.1038/cddiscovery.2015.59>.
- [72] Y. Octavia, C.G. Tocchetti, K.L. Gabrielson, S. Janssens, H.J. Crijs, A.L. Moens, Doxorubicin-induced cardiomyopathy: from molecular mechanisms to therapeutic strategies, *J. Mol. Cell. Cardiol.* 52 (6) (2012) 1213–1225, <https://doi.org/10.1016/j.yjmcc.2012.03.006>.
- [73] A. Minotti, P. Menna, E. Salvatorelli, G. Cairo, L. Gianni, Anthracyclines: molecular advances and pharmacologic developments in antitumor activity and

- cardiotoxicity, *Pharmacol. Rev.* 56 (2) (2004) 185–229, <https://doi.org/10.1124/pr.56.2.6>.
- [74] X. Chen, Y. Zhang, Z. Zhu, H. Liu, H. Guo, C. Xiong, K. Xie, X. Zhang, S. Su, Protective effect of berberine on doxorubicin-induced acute hepatorenal toxicity in rats, *Mol. Med. Rep.* 13 (5) (2016) 3953–3960, <https://doi.org/10.3892/mmr.2016.5017>.
- [75] P.L. Prasanna, K. Renu, A.V. Gopalakrishnan, New molecular and biochemical insights of doxorubicin-induced hepatotoxicity, *Life Sci.* 250 (2020), 117599, <https://doi.org/10.1016/j.lfs.2020.117599>.
- [76] A.J. Favreau-Lessard, H. Blaszyk, M.A. Jones, D.B. Sawyer, I.M. Pinz, Systemic and cardiac susceptibility of immune compromised mice to doxorubicin, *Cardio-Oncology* 5 (1) (2019) 1–10, <https://doi.org/10.1186/s40959-019-0037-6>.
- [77] I.D. Komaritsa, S.N. Baranov, A.P. Grishuk, 4-Thiazolidines, derivatives and analogs: V. arylidene derivatives of isorhodanine, *Chem. Heterocycl. Compd.* 3 (2) (1967) 533–534, <https://doi.org/10.1007/BF00481594>.
- [78] D. Kaminskyy, O. Vasilenko, D. Atamanyuk, A. Gzella, R. Lesyk, Isorhodanine and thiorhodanine motifs in the synthesis of fused thiopyrano[2,3-d][1,3]thiazoles, *Synlett* 10 (2011) 1385–1388, <https://doi.org/10.1055/s-0030-1260765>.
- [79] P.R.O. CrysAlis, Version 1.171.41.93a, Rigaku Oxford Diffraction, Yarnton, U.K., 2020.
- [80] G.M. Sheldrick, SHELXT - integrated space-group and crystal-structure determination, *Acta Crystallogr. A* 71 (2015) 3–8, <https://doi.org/10.1107/S2053273314026370>.
- [81] G.M. Sheldrick, Crystal structure refinement with SHELXL, *Acta Crystallogr. C* 71 (2015) 3–8, <https://doi.org/10.1107/S2053229614024218>.
- [82] L.J. Farrugia, WinGX and ORTEP for windows: an update, *J. Appl. Crystallogr.* 45 (2012) 849–854, <https://doi.org/10.1107/S0021889812029111>.
- [83] O.V. Dolomanov, L.J. Bourhis, R.J. Gildea, J.A.K. Howard, H. Puschmann, OLEX2: a complete structure solution, refinement and analysis program, *J. Appl. Crystallogr.* 42 (2009) 339–341, <https://doi.org/10.1107/S0021889808042726>.
- [84] G.M. Morris, D.S. Goodsell, R.S. Halliday, R. Huey, W.E. Hart, R.K. Belew, A. J. Olson, Automated docking using a Lamarckian genetic algorithm and an empirical binding free energy function, *J. Comput. Chem.* 19 (14) (1998) 1639–1662, [https://doi.org/10.1002/\(SICI\)1096-987X\(19981115\)19:14<1639::AID-JCC10>3.0.CO;2-B](https://doi.org/10.1002/(SICI)1096-987X(19981115)19:14<1639::AID-JCC10>3.0.CO;2-B).
- [85] V.N. Maiorov, G.M. Crippen, Significance of root-mean-square deviation in comparing three-dimensional structures of globular proteins, *J. Mol. Biol.* 235 (2) (1994) 625–634, <https://doi.org/10.1006/jmbi.1994.1017>.
- [86] M. Alisik, S. Neselioglu, O. Erel, A colorimetric method to measure oxidized, reduced and total glutathione levels in erythrocytes, *J. Lab. Med.* 43 (5) (2019) 269–277, <https://doi.org/10.1515/labmed-2019-0098>.
- [87] N. Finiuk, A. Kryshchshyn-Dylevykh, S. Holota, O. Klyuchivska, A. Kozytskiy, O. Karpenko, N. Manko, I. Ivasechko, R. Stoika, R. Lesyk, Novel hybrid pyrrolidinedione-thiazolidinones as potential anticancer agents: synthesis and biological evaluation, *Eur. J. Med. Chem.* 238 (2022), 114422, <https://doi.org/10.1016/j.ejmech.2022.114422>.
- [88] N. Franken, H. Rodermond, J. Stap, J. Haveman, C. Van Bree, Clonogenic assay of cells *in vitro*, *Nat. Protoc.* 1 (5) (2006) 2315–2319, <https://doi.org/10.1038/nprot.2006.339>.
- [89] N. Finiuk, O. Klyuchivska, I. Ivasechko, V. Hreniukh, Y. Ostapiuk, Y. Shalai, R. Panchuk, V. Matyichuk, M. Obushak, R. Stoika, A. Babsky, Proapoptotic effects of novel thiazole derivative on human glioma cells, *Anti Cancer Drugs* 30 (1) (2019) 27–37, <https://doi.org/10.1097/CAD.0000000000000686>.
- [90] L. Borkova, S. Gurska, P. Dzubak, R. Burianova, M. Hajduch, J. Sarek, I. Popa, M. Urban, Lupane and 18 $\alpha$ -oleanane derivatives substituted in the position 2, their cytotoxicity and influence on cancer cells, *Eur. J. Med. Chem.* 121 (2016) 120–131, <https://doi.org/10.1016/j.ejmech.2016.05.029>.
- [91] L. Chen, S. Xu, L. Liu, X. Wen, Y. Xu, J. Chen, J. Teng, Cab45S inhibits the ER stress-induced IRE1-JNK pathway and apoptosis via GRP78/BiP, *Cell Death Dis.* 5 (5) (2014), <https://doi.org/10.1038/cddis.2014.193> e1219–e1219.
- [92] I. Ivasechko, I. Yushyn, P. Roszczenko, J. Senkiv, N. Finiuk, D. Lesyk, S. Holota, R. Czarnomysy, O. Klyuchivska, D. Khylyuk, N. Kashchak, A. Gzella, K. Bielawski, A. Bielawska, R. Stoika, R. Lesyk, Development of novel pyridine-thiazole hybrid molecules as potential anticancer agents, *Molecules* 27 (19) (2022) 6219, <https://doi.org/10.3390/molecules27196219>.